Anlotinib Induces a T Cell–Inflamed Tumor Microenvironment by Facilitating Vessel Normalization and Enhances the Efficacy of PD-1 Checkpoint Blockade in Neuroblastoma

Yudong Su[1,2,3,4], Bingying Luo[5], Yao Lu[5], Daowei Wang[1,2,3,4], Jie Yan[1,2,3,4], Jian Zheng[5], Jun Xiao[5], Yangyang Wang[1,2,3,4], Zhenyi Xue[5], Jie Yin[5], Peng Chen[1,2,3,6], Long Li[1,2,3,4,5], and Qiang Zhao[1,2,3,4]

ABSTRACT

Purpose: Anlotinib has achieved good results in clinical trials of a variety of cancers. However, the effects of anlotinib on the tumor microenvironment (TME) and systemic immunity have not been reported. There is an urgent need to identify the underlying mechanism to reveal new opportunities for its application in neuroblastoma (NB) and other cancers. Understanding the mechanism will hopefully achieve the goal of using the same method to treat different cancers.

Experimental Design: This study used bioinformatics, NB syngeneic mouse models, flow cytometry, RNA-seq, and immunofluorescence staining to explore the mechanisms of anlotinib on the TME, and further explored anlotinib-containing combination treatment strategies.

Results: We proved that anlotinib facilitates tumor vessel normalization at least partially through $CD4^+$ T cells, reprograms the immunosuppressive TME into an immunostimulatory TME, significantly inhibits tumor growth, and effectively prevents systemic immunosuppression. Moreover, the combination of anlotinib with a PD-1 checkpoint inhibitor counteracts the immunosuppression caused by the upregulation of PD-L1 after monotherapy, extends the period of vascular normalization, and finally induces NB regression.

Conclusions: To our knowledge, this study is the first to dynamically evaluate the effect of a multitarget antiangiogenic tyrosine kinase inhibitor on the TME. These findings have very important clinical value in guiding the testing of related drugs in NB and other cancers. Based on these findings, we are conducting a phase II clinical study (NCT04842526) on the efficacy and safety of anlotinib, irinotecan, and temozolomide in the treatment of refractory or relapsed NB, and hopefully we will observe patient benefit.

Introduction

Neuroblastoma (NB) is derived from embryonic neural crest cells and has the characteristics of abundant blood vessels, rapid growth, and early metastasis. It is the most common extracranial solid tumor and the second leading cause of death related to malignant tumors in children (1). The clinical features and outcomes of NB are highly heterogeneous: a small number of cases resolve spontaneously, but most of them are already at an advanced stage at the time of diagnosis. Despite comprehensive treatment measures such as surgery, high-dose chemotherapy, radiotherapy, autologous stem cell transplantation, and anti-GD2 therapy, the cure rate is still less than 50%, and there is an urgent clinical need for new and efficient treatment methods (2).

With the approval of programmed cell death receptor 1 (PD-1) inhibitors, programmed cell death ligand 1 (PD-L1) inhibitors, cytotoxic T lymphocyte-associated antigen 4 (CTLA-4) inhibitors, and other related drugs, immune-checkpoint inhibitors (ICI) have become a research hotspot in the field of oncology and have substantially improved the prognosis of some patients (3). However, 50% to 80% of patients with cancer, including patients with NB, do not benefit from these treatments, and many patients will experience adverse reactions (4). Some tumor cells have a low mutation load and lack major histocompatibility complex I (MHC-I) expression, leading to low immunogenicity and preventing T cells from recognizing them (5). However, this alone is insufficient to fully explain the lack of response to treatment in most patients, nor does the differences in the expression of immune-checkpoint proteins (6). Indeed, a reliable biomarker that accurately predicts the clinical response of patients to immunotherapy is currently unavailable. The tumor microenvironment (TME), which is characterized by a low oxygen level, low pH, and high interstitial pressure, may reduce the effectiveness of almost all types of anticancer therapies, including immunotherapy (7). The TME is composed of blood vessels, lymphatic vessels, various stromal cells, and immune cells, all of which are wrapped in an extracellular matrix.

[1]Tianjin Medical University Cancer Institute and Hospital, National Clinical Research Center for Cancer, Tianjin, China. [2]Key Laboratory of Cancer Prevention and Therapy, Tianjin, China. [3]Tianjin Clinical Research Center for Cancer, Tianjin, China. [4]Department of Pediatric Oncology, Tianjin Cancer Institute and Hospital, Tianjin Medical University, Tianjin, China. [5]Key Laboratory of Immune Microenvironment and Diseases of Educational Ministry of China, The Province and Ministry Cosponsored Collaborative Innovation Center for Medical Epigenetics, Department of Immunology, Tianjin Medical University, Tianjin, China. [6]Department of Thoracic Oncology, Tianjin Cancer Institute and Hospital, Tianjin Medical University, Tianjin, China.

Note: Supplementary data for this article are available at Clinical Cancer Research Online (http://clincancerres.aacrjournals.org/).

Corresponding Authors: Qiang Zhao, Department of Pediatric Oncology, Tianjin Medical University Cancer Institute and Hospital, National Clinical Research Center for Cancer, Tianjin Key Laboratory of Cancer Prevention and Therapy, Tianjin Clinical Research Center for Cancer, Tianjin 300060, China. Phone: 86-22-2334-0123; E-mail: zhaoqiang@tjmuch.com; and Long Li, Key Laboratory of Immune Microenvironment and Diseases of Educational Ministry of China, The Province and Ministry Cosponsored Collaborative Innovation Center for Medical Epigenetics, Department of Immunology, Tianjin Medical University, Tianjin, 300070, China. Phone: 86-22-2334-0123; E-mail: Long.Li@tmu.edu.cn

Clin Cancer Res 2022;28:793–809

doi: 10.1158/1078-0432.CCR-21-2241

This open access article is distributed under Creative Commons Attribution-NonCommercial-NoDerivatives License 4.0 International (CC BY-NC-ND).

©2021 The Authors; Published by the American Association for Cancer Research

Translational Relevance

The findings of multiple preclinical studies have provided evidence for the efficacy of combining antiangiogenic therapy with immune-checkpoint inhibitors. A phase I clinical study (NCT03628521) of anlotinib combined with sintilimab as the first-line treatment of advanced non–small cell lung cancer (NSCLC) showed encouraging efficacy, tolerability, and safety. Here, we proved that anlotinib facilitates tumor vessel normalization at least partially through $CD4^+$ T cells, reprograms the immunosuppressive tumor microenvironment (TME) into an immunostimulatory TME, significantly inhibits tumor growth, and effectively prevents systemic immunosuppression. Moreover, the combination of anlotinib with a PD-1 checkpoint inhibitor counteracts the immunosuppression caused by the upregulation of PD-L1 after monotherapy, extends the period of vascular normalization, and finally induces neuroblastoma (NB) regression. Based on these findings, we are conducting a phase II clinical study (NCT04842526) on the efficacy and safety of anlotinib, irinotecan, and temozolomide in the treatment of refractory or relapsed NB, and hopefully we will observe patient benefit.

Many studies have shown that the various components of the TME are highly abnormal compared with normal tissues, which aggravates tumor progression and treatment resistance (8). Therefore, facilitating TME normalization can improve the effect of anticancer therapies (such as chemotherapy, radiotherapy, targeted therapy, and immunotherapy; ref. 9). Therefore, we focused on tumor blood vessels, which are an important part of the TME. Vascular abnormalities are a hallmark of most solid tumors, and these abnormalities stem from the increased levels of proangiogenic factors such as vascular endothelial growth factor (VEGF) and angiopoietin 2 (ANGPT2). The use of drugs targeting these factors can improve the immunotherapy response. One explanation is that these drugs can facilitate vessel normalization to increase the infiltration of immune effector cells; namely, they can transform the immunosuppressive TME into an immune-enhancing TME (6). Notably, ICIs can facilitate vessel normalization in breast cancer models through a mechanism mediated by $CD4^+$ T cells in an IFNγ-dependent manner, and mutual regulation of tumor vascular normalization and immunostimulatory reprogramming has been observed (10). However, researchers have not yet determined whether the ICI-mediated vascular normalization theory is suitable for other cancer models.

Bevacizumab is a humanized VEGF antibody that has been approved by the Food and Drug Administration (FDA) for the treatment of a variety of cancers (11). Because it is a single-target antiangiogenic drug, it has no inhibitory effect on the tumor itself; bevacizumab monotherapy does not result in significant improvement in prognosis, and thus it is often used in combination with other treatments as an adjuvant therapy. A phase II clinical study of its combination with irinotecan and temozolomide in the treatment of patients with refractory and relapsed NB showed that the combination therapy was well tolerated, but it did not improve the response rate (12). Anlotinib is a new, orally administered small-molecule multitarget tyrosine kinase inhibitor that was independently developed in China; it strongly inhibits vascular endothelial growth factor receptor (VEGFR), fibroblast growth factor receptor (FGFR), platelet-derived growth factor receptor (PDGFR), and c-KIT, and thus it acts on both the TME and the tumor itself (13). The results of a multicenter, randomized, double-blind, placebo-controlled phase III clinical study of anlotinib as a third-line treatment for advanced non–small cell lung cancer (NSCLC) showed that the overall survival (OS) and progression-free survival (PFS) times of the anlotinib group were significantly longer than those of the placebo group (14). Therefore, it was officially approved by the China Food and Drug Administration on May 9, 2018, for the third-line treatment of patients with advanced NSCLC. It is currently the only effective monotherapy among antiangiogenic drugs approved for advanced NSCLC, and it has controllable adverse reactions that are well tolerated by patients. First-line and second-line combination strategies, including anlotinib, have broad prospects. Anlotinib alone has also achieved good results in clinical trials of advanced soft tissue sarcoma (15), medullary thyroid carcinoma (16), metastatic renal cell carcinoma (17), and other cancers (13). However, the effects of anlotinib on the TME and systemic immunity have not been reported, and it has not been used in patients with NB. There is an urgent need to identify the underlying mechanism to reveal new opportunities for its application in NB and other cancers. Understanding the mechanism will hopefully achieve the goal of using the same method to treat different cancers. This study used syngeneic mouse models to explore the effects and mechanisms of anlotinib on the NB TME and systemic immunity and further explored anlotinib-containing combination treatment strategies.

Materials and Methods

Bioinformatic analysis

NB data analyzed in this study were obtained from GSE62564. Lung adenocarcinoma (LUAD) data analyzed in this study were obtained from GSE68465. The bioinformatic analysis process and code were as described previously (10). Briefly, the pheatmap R package was used to perform the cluster analysis and draw heatmaps. The survival and survminer R packages were used for the survival analysis and to generate Kaplan–Meier curves. The differentially expressed genes (DEG) were identified in the two groups of patients using the limma R package (18). Gene set enrichment analysis (GSEA) was performed using the clusterProfiler R package (19).

Cell lines and cell culture

975A2 and 9464D cells (gifts from Dr. Rimas Orentas at Seattle Children's Research Institute) were cultured in high-glucose DMEM (Gibco) containing 10% FBS (BI) and 100 IU/mL penicillin/streptomycin (Gibco). Both cell lines were grown in a humidified incubator at 37°C with 5% CO_2 and confirmed to be negative for *mycoplasma* contamination every month by PCR. Cell lines were used within 20 passages of thawing and continuously cultured for less than six months. Both cell lines were derived from spontaneous NB in the adrenal glands of TH-MYCN transgenic mice on a C57BL/6 background. TH-MYCN transgenic mice spontaneously develop NB, and these NB tumors have strong histologic and genetic similarities to human NB (20). The TH-MYCN mouse model closely recapitulates the human disease and mainly resembles high-risk *MYCN*-amplified NB tumors (21). The transplantable TH-MYCN model represents a relevant model for the development of novel immunocombinatorial approaches for patients with NB (22, 23).

Construction of OVA-flag-GFP-975A2/9464D cell lines

The recombinant lentiviral vector pLV-OVA-Flag-IRES-GFP was obtained from Dr. Deqing Hu at Tianjin Medical University. The EndoFree Plasmid Kit (12362, Qiagen) was used to prepare the packaging plasmid psPAX2 and the envelope plasmid pMD2.G (both

from Addgene). The three plasmids were cotransfected into 293T cells with polyethylenimine (PEI; 23966, Polysciences) to prepare the virus, and then 975A2/9464D cells were infected with the virus. Monoclonal cells expressing OVA-Flag-GFP were collected by fluorescence activated cell sorting and expanded into cell lines. The expression of the OVA protein was confirmed by western blot, and the expression of GFP was confirmed by observing cells with an OLYMPUS CKX53 microscope.

NB syngeneic mouse models

Female C57BL/6 mice and athymic nude mice (6 to 8 weeks old) were purchased from SPF (Beijing) Biotechnology Co., Ltd. 975A2/975A2-OVA (2×10^6) and 9464D/9464D-OVA (1×10^6) tumor cells were subcutaneously implanted into the right back of C57BL/6 and nude mice. When the mean tumor volume (TV) reached 30 to 50 mm^3, the mice were randomized into treatment groups ($n = 5$–10 mice per group). At the time point of the dynamic analysis, three mice from each group were used for mechanistic analyses. TV was calculated as TV (mm^3) $= \pi/6 \times$ length $\times$ width $\times$ height. We measured the TV every three days. For survival experiments, the animals were sacrificed when the TV exceeded 2,500 mm^3 or it was expected to surpass 2,500 mm^3 before the next measurement.

Drugs and antibodies

Anlotinib was provided by Chia Tai Tianqing Pharmaceutical Group Co., Ltd. The murine PD-1 antibody (clone RMP1-14) and its isotype-matched control antibody (clone 2A3), CD4 antibody (clone GK1.5), and isotype-matched control antibody (clone LTF-2), CD8 antibody (clone 53-6.7) and isotype-matched control antibody (clone 2A3) were all purchased from Bio X Cell.

In vivo treatment

Anlotinib was intragastrically administered to mice for 9 or 21 consecutive days, and the PD-1 antibody or its isotype-matched control antibody (both 10 mg/kg) was injected intraperitoneally every three days. To deplete $CD4^+$ or $CD8^+$ T cells, mice carrying early established tumors were injected intraperitoneally with the corresponding antibody or isotype-matched control antibody (all 10 mg/kg) every three days starting six days before anlotinib treatment.

RNA-seq analysis

After nine days of anlotinib treatment, three mice each from the treatment group and the vehicle group were sacrificed, and the tumors were snap-frozen in liquid nitrogen immediately after resection. RNA extraction and RNA-seq analysis were performed by Beijing Novogene Co., Ltd. One microgram of total RNA per sample was used as input material for the RNA sample preparations. Sequencing libraries were generated using the NEBNext UltraTM RNA Library Prep Kit for Illumina (NEB, USA) following the manufacturer's recommendations. The library fragments were purified with the AMPure XP system (Beckman Coulter), and library quality was assessed using the Agilent Bioanalyzer 2100 system. The library preparations were sequenced on an Illumina NovaSeq platform, and 150 bp paired-end reads were generated. The index of the reference genome was built using Hisat2 v2.0.5 and paired-end clean reads were aligned to the reference genome using Hisat2 v2.0.5. Next, featureCounts v1.5.0-p3 was used to count the read numbers mapped to each gene. Then, fragments per kilobase per million (FPKM) of each gene were calculated based on the length of the gene and read count mapped to this gene. The differential expression analysis was performed using the DESeq2 R package (1.16.1). The resulting *P* values were adjusted using the Benjamini and Hochberg's approach for controlling the false discovery rate. Genes with an adjusted $P < 0.05$ and $|\log2 \text{ (fold change)}| > 0.5$ identified by DESeq2 were considered differentially expressed. Gene Ontology (GO) enrichment analysis of DEGs was implemented using the clusterProfiler R package. GO terms with corrected *P* less than 0.05 were considered significantly enriched in DEGs. The local version of the GSEA tool http://www.broadinstitute.org/gsea/index.jsp was used for GSEA.

Flow cytometry

Tumors were cut into small fragments (approximately 1 mm^3), incubated for 1 hour with Hank's solution containing 0.5 mg/mL collagenase type III, 0.1 mg/mL dispase II, and 0.1 mg/mL DNase at 37°C on a constant temperature shaker, and then filtered through a 70-μm cell strainer to obtain a single-cell suspension. A 30% Percoll separation solution was used for density gradient centrifugation to remove fibrous tissue, and then ACK lysis buffer was used to lyse red blood cells. The cells were incubated for 10 minutes at 4°C with fixable viability dye (423106, BioLegend, 1:1,000) and then incubated for 15 minutes at 4°C with anti-mouse Fc-block CD16/32 antibody (clone 93, BioLegend, 1:200). Cell membrane proteins were subsequently analyzed by staining with antibodies for 40 minutes at 4°C. For intracellular staining, the cells were fixed, permeabilized, and then incubated with the antibodies at 4°C for 40 minutes. For cytokine staining, the cells were incubated for 5 hours with a cell activation cocktail (BioLegend, 1:500) in DMEM containing 10% FBS at 37°C and then stained as described above. The following antibodies against mouse antigens were used: anti-CD45 (clone 30-F11), anti-CD3 (clone 145-2C11), anti-CD4 (clone GK1.5), anti-CD8 (clone 53-6.7), anti-CD11b (clone M1/70), anti-CD11c (clone N418), anti-CD19 (clone 1D3/CD19), anti-CD25 (clone PC61), anti-CD31 (clone 390), anti-NK1.1 (clone PK136), anti-Gr1 (clone RB6-8C5), anti-F4/80 (clone BM8), anti-CD206 (clone C068C2), anti-CD80 (clone 16-10A1), anti-CD86 (clone GL-1), anti-Arg1 (clone A1exF5), anti-Foxp3 (clone 150D), anti-Ki67 (clone 11F6), anti-TNFα (clone MP6-XT22), anti-IFNγ (clone XMG1.2), anti-GzmB (clone QA16A02), anti–PD-1 (clone 29F.1A12), anti-Lag3 (clone C9B7W), anti-Tim3 (clone B8.2C12), anti–PD-L1 (clone 10F.9G2), anti-MHC-II (clone M5/114.15.2), anti-H-2 (clone M1/42), and anti-$H\text{-}2K^b$ bound to SIINFEKL (clone 25-D1.16; all from BioLegend); anti-iNOS (clone CXNFT, eBioscience); and anti-β_2M (clone S19.8, BD Biosciences). Data were acquired using a BD LSRFortessa cytometer (BD Biosciences) and analyzed with FlowJo v10.4 software.

Immunofluorescence staining

The excised tumor tissue blocks were embedded in optimal cutting temperature (OCT) compound and quickly frozen in liquid nitrogen. Sections with thicknesses of 5 μm were cut on a Leica CM1850 cryotome. The slides were fixed with 4% paraformaldehyde solution for 15 minutes and then blocked with PBS containing 5% goat serum (Sangon Biotech), 1% BSA (BI), and 0.3% Triton X-100 (Solarbio) for 1 hour at 20°C. Primary antibodies in blocking solution were added and incubated overnight at 4°C. Secondary antibodies in blocking solution were added and incubated for 1 hour at 20°C. Sections were then washed and mounted with DAPI. The primary antibodies included anti-CD31, anti-α-smooth muscle actin (α-SMA), and anti-carbonic anhydrase IX (CA-IX; all from Abcam). The secondary antibodies included Alexa Fluor 488–conjugated goat anti-rabbit and Alexa Fluor 555–conjugated goat anti-rat (both from Cell Signaling Technology). Stained sections were stored at −20°C and visualized using a Carl Zeiss Axio imager A2 microscope. For the quantification

of pericyte coverage, vessels were counted manually in five independent fields at ×400 magnification, and the percentage of vessels covered by pericytes was calculated as the number of $CD31^+$ cells attached by α-SMA^+ cells divided by the number of $CD31^+$ cells. Perfusion efficiency was quantified as the number of $CD31^+lectin^+$ cells divided by the number of $CD31^+$ cells. The degree of vascular leakage was quantified as the number of $CD31^+dextran^+$ cells divided by the number of $CD31^+$ cells. Hypoxia levels were quantified as the number of $CA\text{-}IX^+$ cells divided by the number of $DAPI^+$ cells. Fluorescence photos were analyzed with ImageJ (US NIH) and Photoshop (Adobe Systems Inc) software.

Tumor vascular perfusion and leakage evaluation

For the evaluation of vessel perfusion and leakiness, mice were administered 1 mg of 70-kDa lysine fixable fluorescein-labeled dextran (Thermo Fisher) and 50 μg of DyLight 649-labeled tomato lectin (Lycopersicon esculentum; Vector Labs) via tail-vein injection. After 10 minutes (to allow the dye to circulate), the mice were euthanized, and a vertical inline incision along the sternum was made to expose the heart and lungs. Whole-animal perfusion was performed. An incision was made in the right atrium, and 10 mL of PBS containing 2 mmol/L EDTA (Solarbio) was injected through the left ventricle to remove intravascular dye. The tumors were embedded in OCT compound after resection, and the immunofluorescence staining procedure was performed as described above.

Study approval

All mouse experimental procedures were performed in accordance with the guidelines of the NIH Guide for Care and Use of Animals, and the experimental protocol was approved by the Institutional Animal Care and Research Advisory Committee of Tianjin Medical University.

Statistical methods

Sample sizes are indicated in figures or figure legends and refer to the number of mice. The data were analyzed with Prism 8 software (GraphPad) or the R programming language (v4.0.3) supported by the R Foundation for Statistical Computing. For experiments with two groups, the statistical analysis was performed using two-tailed Student *t* test. In some experiments involving multiple groups, statistical significance was determined using two-way analysis of variance (ANOVA). Survival analyses were evaluated by constructing Kaplan–Meier curves and using the log-rank (Mantel–Cox) test. The Pearson correlation coefficient was calculated to analyze the correlation between tumor weight and the proportion of immune cells. Differences with *P* values less than 0.05 were considered statistically significant.

Data availability

All data in this study are available upon reasonable request. The RNA-seq data have been submitted to the Gene-Expression Omnibus (GEO) under accession number GSE179550.

Results

Good prognosis-related angiogenesis genes (GPAG) are associated with vessel normalization and T-cell activation in patients with NB

The GEO database was used to explore the genes related to the angiogenesis in NB patients. Among 377 genes, 156 were positively correlated with OS, and 52 were negatively correlated with OS; these genes were defined as GPAGs and poor prognosis-related angiogenesis genes (PPAG), respectively (Supplementary Table S1A and S1B), which can be used to stratify patients according to prognosis (**Fig. 1A** and **B**). The results indicate that angiogenesis may play different roles in NB tumor development depending on molecular backgrounds. The GPAGs were mostly related to positive regulation of vascular-associated smooth muscle cell proliferation, migration, contraction, and regulation of leukocyte adhesion to vascular endothelial cells (EC) and other pathways associated with vascular normalization (**Fig. 1C**; Supplementary Table S2A and S2B). Pericytes and smooth muscle cells have similar gene-expression programs and are considered to be developmentally related (24). Pericyte recruitment and proliferation are highly regulated processes that are essential to vascular normalization (10). Therefore, GPAGs may be a molecular marker for vascular normalization. In contrast, the PPAGs were mostly related to negative regulation of smooth muscle cell differentiation and positive regulation of the VEGFR signaling pathway and other pathways opposite to vascular normalization (**Fig. 1C**; Supplementary Table S2A and S2C). GSEA showed that GPAGs are associated with the adaptive immune response, especially T-cell activation (**Fig. 1D**; Supplementary Table S3). The above results showed that GPAGs are associated with vessel normalization and T-cell activation in patients with NB. An analysis of patients with LUAD also supported the conclusions described above (Supplementary Fig. S1; Supplementary Tables S4–S6).

Anlotinib significantly inhibits tumor growth in 975A2 and 9464D syngeneic mouse models and reprograms the NB immunostimulatory microenvironment

A reasonable dose and administration time of antiangiogenic drugs induce the normalization of tumor vessels by inhibiting tumor angiogenesis, improving the coverage of pericytes and promoting vessel maturation. The normal vascular network directly promotes the delivery of antitumor drugs and the adhesion, infiltration and activity of immune cells (6). Therefore, the dose and exposure time of anlotinib that normalizes tumor vessels must be determined. We first tested the therapeutic effect of different doses of anlotinib in NB syngeneic mouse models. Compared with vehicle treatment, both 6 and 12 mg/kg anlotinib treatments significantly inhibited tumor growth and prolonged survival, but no significant difference was observed between the two anlotinib groups (**Fig. 2A–D**). Then, we performed RNA-seq of tumor tissues treated with vehicle ± anlotinib (6 mg/kg) for 9 days and analyzed the DEGs by GO analysis and GSEA to explore the mechanism of anlotinib in the treatment of NB. The 6 mg/kg treatment significantly upregulated genes involved in immune-related pathways such as adaptive immune response, T-cell activation, regulation of IFNγ production, lymphocyte chemotaxis, migration and adhesion, and cytokine receptor activity and significantly downregulated genes involved in angiogenesis-related pathways such as cellular response to VEGF stimulus and blood vessel EC proliferation involved in sprouting angiogenesis (**Fig. 2E–H**; Supplementary Fig. S2A–S2D). The heatmaps of DEGs showed that genes related to T-cell activation, immune cell adhesion (*Selp, Madcam1*, and *Icam1*), and immune cell migration (*Cxcl9, Cxcl10*, and *Cxcr3*) were significantly upregulated, whereas genes related to angiogenesis (*Angpt2, Pdgfa*, and *Pdgfb*) were significantly downregulated in the 6 mg/kg treatment group (**Fig. 2I–L**; Supplementary Fig. S2E–S2H). We further confirmed the key role of T-cell activation in the therapeutic effect of anlotinib on NB by conducting experiments with nude mice. The therapeutic effect of anlotinib on nude mice was obviously not as good as that on C57BL/6 mice with normal immunity (**Fig. 2M–P**).

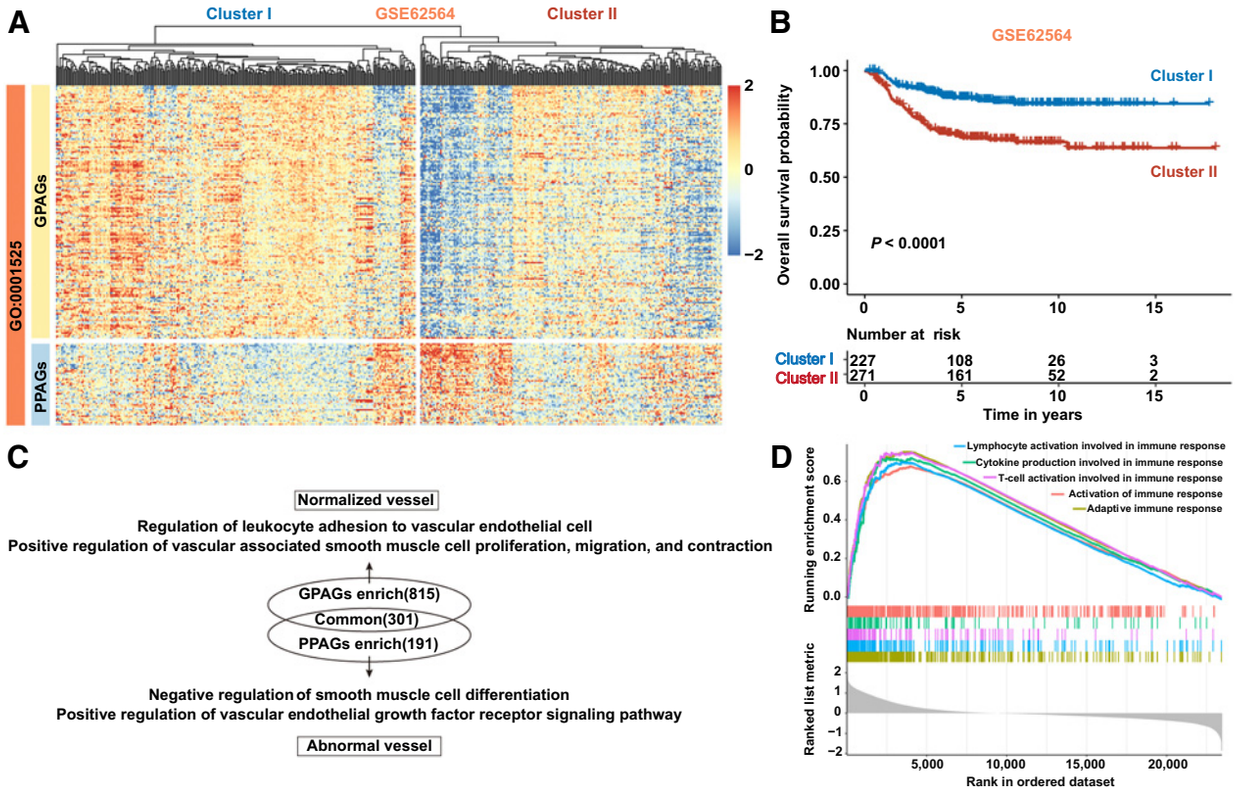

Figure 1.

GPAGs are associated with vessel normalization and T-cell activation in patients with NB. **A** and **B,** The hierarchical clustering analysis of angiogenesis-related genes (GO: 0001525) associated with the prognosis showed two clusters of patients with differences in OS. The color scale represents row z-scores (**A**). **C,** GO terms that associated with GPAGs and PPAGs. The GPAGs were mostly related to positive regulation of vascular-associated smooth muscle cell proliferation, migration, contraction, and regulation of leukocyte adhesion to vascular EC and other pathways associated with vascular normalization. The PPAGs were mostly related to negative regulation of smooth muscle cell differentiation and positive regulation of the VEGFR signaling pathway and other pathways opposite to vascular normalization. The number of pathways is shown in parentheses. **D,** T-cell activation, activation of immune response, and adaptive immune response and other pathways analyzed by GSEA of GPAGs were significantly upregulated. Log-rank test (**B**).

Anlotinib significantly impairs tumor angiogenesis and normalizes the remaining blood vessels, but a concomitant period of vascular normalization occurs

We then dynamically analyzed the features of the tumor vessels after anlotinib treatment (6 mg/kg) by performing immunofluorescence staining (days 9 and 21) as described in Supplementary Fig. S3A. To assess vascular maturation, we visualized pericytes by α-SMA immunostaining, evaluated vascular leakiness by fluorescein-labeled dextran, detected vascular perfusion by fluorescein-labeled lectin, and observed hypoxia of the TME by CA-IX immunostaining in NB syngeneic mouse models. After 9 days of anlotinib treatment, (i) the tumor vessel length was longer than that in the vehicle group; (ii) the number of microvessels was reduced; (iii) the coverage of pericytes and vascular perfusion was significantly increased; (iv) vascular leakage was reduced; and (v) hypoxia was alleviated (**Fig. 3A–J**). The RNA-seq results showed that anlotinib treatment significantly upregulated smooth muscle cell proliferation-related genes (Supplementary Fig. S3B) and enriched vascular normalization-related pathways such as myofilament, α-actinin binding, myosin filament, and structural constituent of muscle on day 9 (Supplementary Fig. S3C). Notably, compared with that in the day 9 treatment group, no significant difference in the number and length of tumor vessels was observed, but the coverage of pericytes and vascular perfusion was decreased, and vascular leakage was increased. We found that hypoxia was aggravated in the day 21 monotherapy group (**Fig. 3A–J**) as well. Based on these results, anlotinib significantly impairs tumor angiogenesis and normalizes the remaining blood vessels, but a concomitant period of vascular normalization is observed.

Anlotinib significantly reprograms the NB immunostimulatory microenvironment, but it is affected by the concomitant period of vascular normalization

Then, we dynamically compared the number and function of tumor-infiltrating immune cells between the 6 mg/kg treatment group and the vehicle group by flow cytometry (days 9 and 21). The proportions and densities of tumor-infiltrating $CD45^+$ immune cells as well as $CD4^+$ and $CD8^+$ T cells were significantly increased; the proportions of TAMs and neutrophils decreased significantly (**Fig. 4A–C**); the abilities of $CD4^+$ and $CD8^+$ T cells to secrete IFNγ, TNFα, and GzmB were significantly enhanced (**Fig. 4D–H**); the proportion of M1 tumor-associated macrophages (TAM) increased; and the proportion of M2 TAMs decreased in the treatment group on day 9 (**Fig. 4I** and **J**). The density of TAMs, their secretion of TNFα, and expression of costimulatory molecules (CD80 and CD86) were significantly increased, and the expression of Arginase 1 (Arg1) was significantly reduced (**Fig. 4C** and **K–N**). RNA-seq results also showed

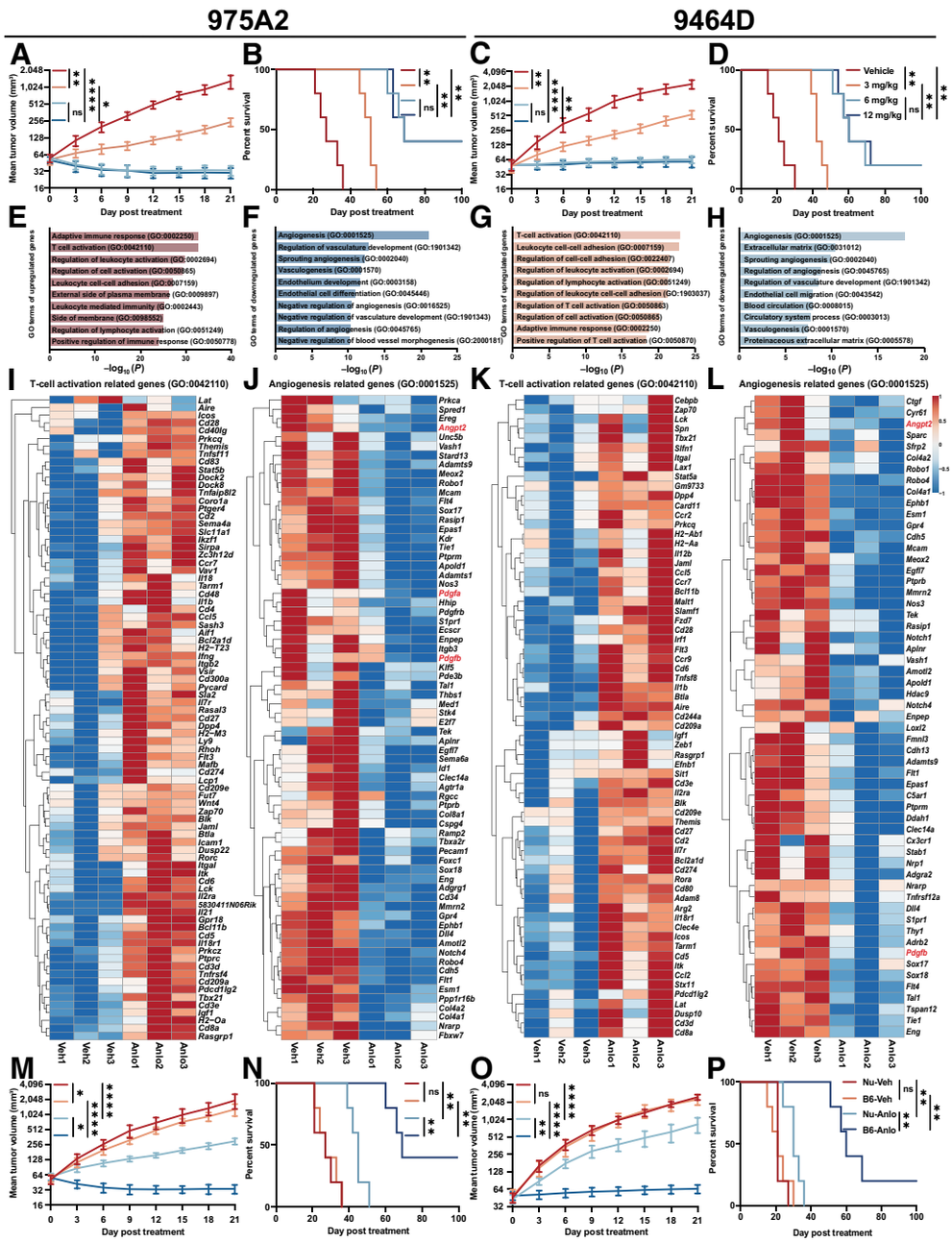

Figure 2.

Anlotinib significantly inhibits tumor growth in 975A2 and 9464D syngeneic mouse models and reprograms the NB immunostimulatory microenvironment. **A–D,** Tumor growth curves and survival curves of 975A2 and 9464D syngeneic mouse models treated with different doses of anlotinib for 21 days as described in Supplementary Fig. S3A ($n = 5$ per group). Median (50%) survival (after treatment): vehicle, 27 days; 3 mg/kg, 51 days; 6 mg/kg, 69 days; and 12 mg/kg, 69 days (**B**). Median (50%) survival (after treatment): vehicle, 21 days; 3 mg/kg, 42 days; 6 mg/kg, 60 days; and 12 mg/kg, 60 days (**D**). **E–L,** RNA-seq expression analysis of tumor tissues from NB syngeneic mouse models treated with vehicle ± anlotinib (6 mg/kg) for 9 days as described in Supplementary Fig. S3A and genes differentially expressed were selected based on the following criteria: adjusted $P < 0.05$ and $|\log2 \text{ (fold change)}| > 0.5$. The top 10 GO terms of DEGs are shown with −log10 (P value) ($n = 3$ per group, **E–H**). Heatmaps of DEGs related to T-cell activation (GO: 0042110) and angiogenesis (GO: 0001525) and the color scale represents row z-scores ($n = 3$ per group, **I–L**). **M–P,** Tumor growth curves and survival curves of vehicle ± anlotinib (6 mg/kg) in nude mouse and C57BL/6 mouse tumor-bearing models ($n = 5$ per group). Median (50%) survival (after treatment): nude-vehicle, 27 days; C57BL/6-vehicle, 27 days; Nude-Anlo, 45 days; and C57BL/6-Anlo, 69 days (**N**). Median (50%) survival (after treatment): nude-vehicle, 21 days; C57BL/6-vehicle, 21 days; nude-Anlo, 30 days; and C57BL/6-Anlo, 60 days (**P**). Error bars represent the mean ± SEM; *, $P < 0.05$; **, $P < 0.01$; ***, $P < 0.001$; ****, $P < 0.0001$, two-way ANOVA (**A**, **C**, **M,** and **O**), log-rank test (**B**, **D**, **N**, and **P**).

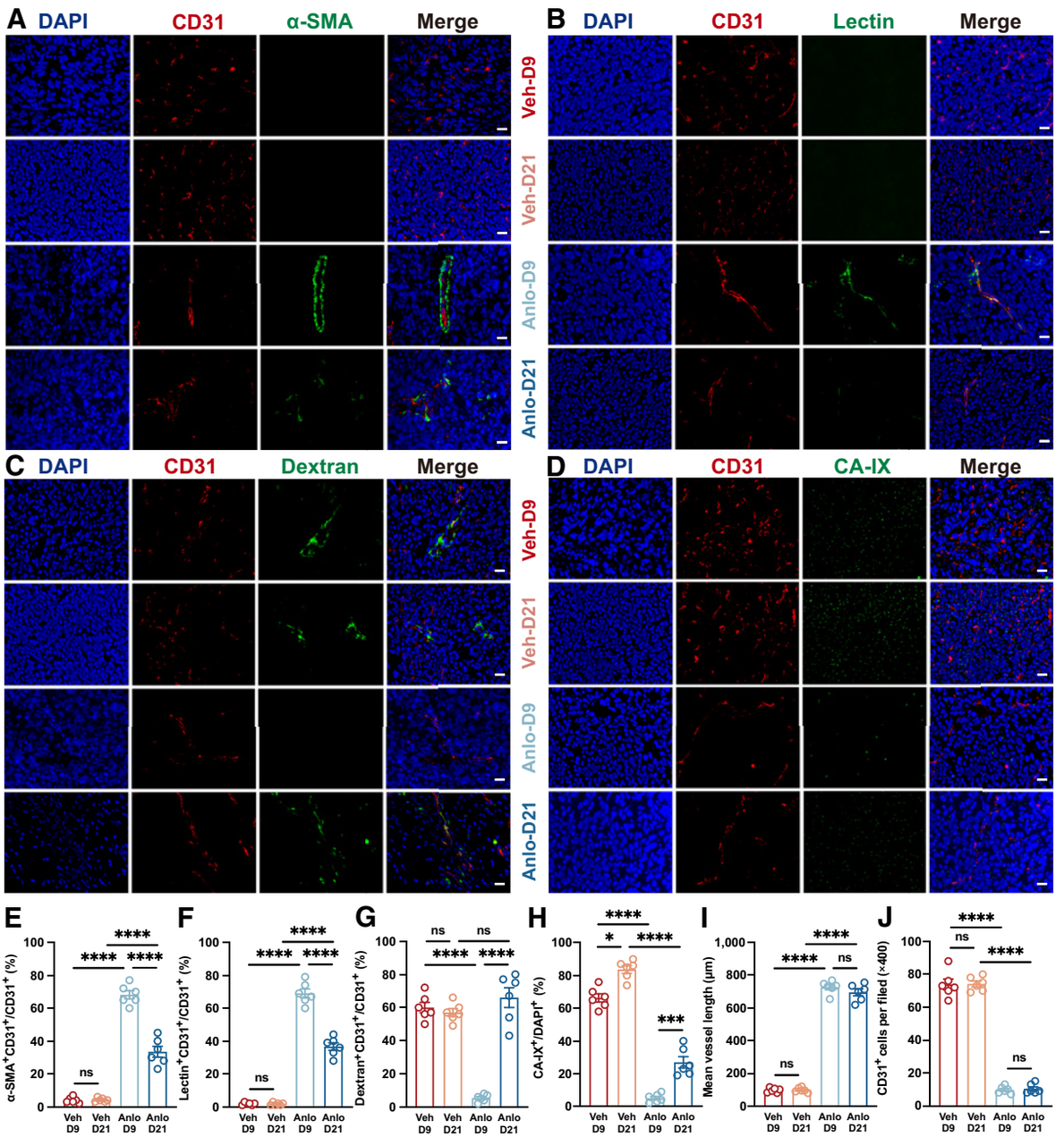

Figure 3.

Anlotinib significantly impairs tumor angiogenesis and normalizes the remaining blood vessels, but a concomitant period of vascular normalization occurs. **A–D,** Representative immunofluorescence images of CD31 (red), α-SMA, lectin, dextran and CA-IX (green), and DAPI (blue) staining in tumor tissues from NB syngeneic mouse models treated with vehicle ± anlotinib (6 mg/kg) for 9 days and 21 days as described in Supplementary Fig. S3A. Scale bars, 100 μm. **E–J,** Quantitation results of immunofluorescent images (**A–D**). Relative proportions of α-SMA$^+$ pericyte-covered blood vessels (**E**), lectin$^+$ blood vessels (**F**), dextran$^+$ blood vessels (**G**), and CA-IX$^+$ cells (**H**) in NB syngeneic mouse models treated with vehicle ± anlotinib (6 mg/kg) for 9 and 21 days as described in Supplementary Fig. S3A. Relative tumor vessel length (**I**) and number of CD31$^+$ cells (**J**) in NB syngeneic mouse models treated with vehicle ± anlotinib (6 mg/kg) for 9 days and 21 days as described in Supplementary Fig. S3A. Each dot indicates one tumor and represents the average of five images. $n = 6$ per group, including 975A2 ($n = 3$) and 9464D ($n = 3$). Error bars represent the mean ± SEM; *, $P < 0.05$; **, $P < 0.01$; ***, $P < 0.001$; ****, $P < 0.0001$, two-way ANOVA (**E–J**).

that the DEGs related to macrophage activation, chemotaxis, migration, and antigen processing and presentation were significantly upregulated in the treatment group on day 9 (Supplementary Fig. S3D and S3E). The density of dendritic cells (DC) and their expression of MHC-II and costimulatory molecules (CD80 and CD86) were increased significantly (**Fig. 4C** and **O–Q**). The expression levels of MHC-I and MHC-II in NB cells were significantly increased in the treatment group on day 9 (**Fig. 4R–T**). However, we did not detect

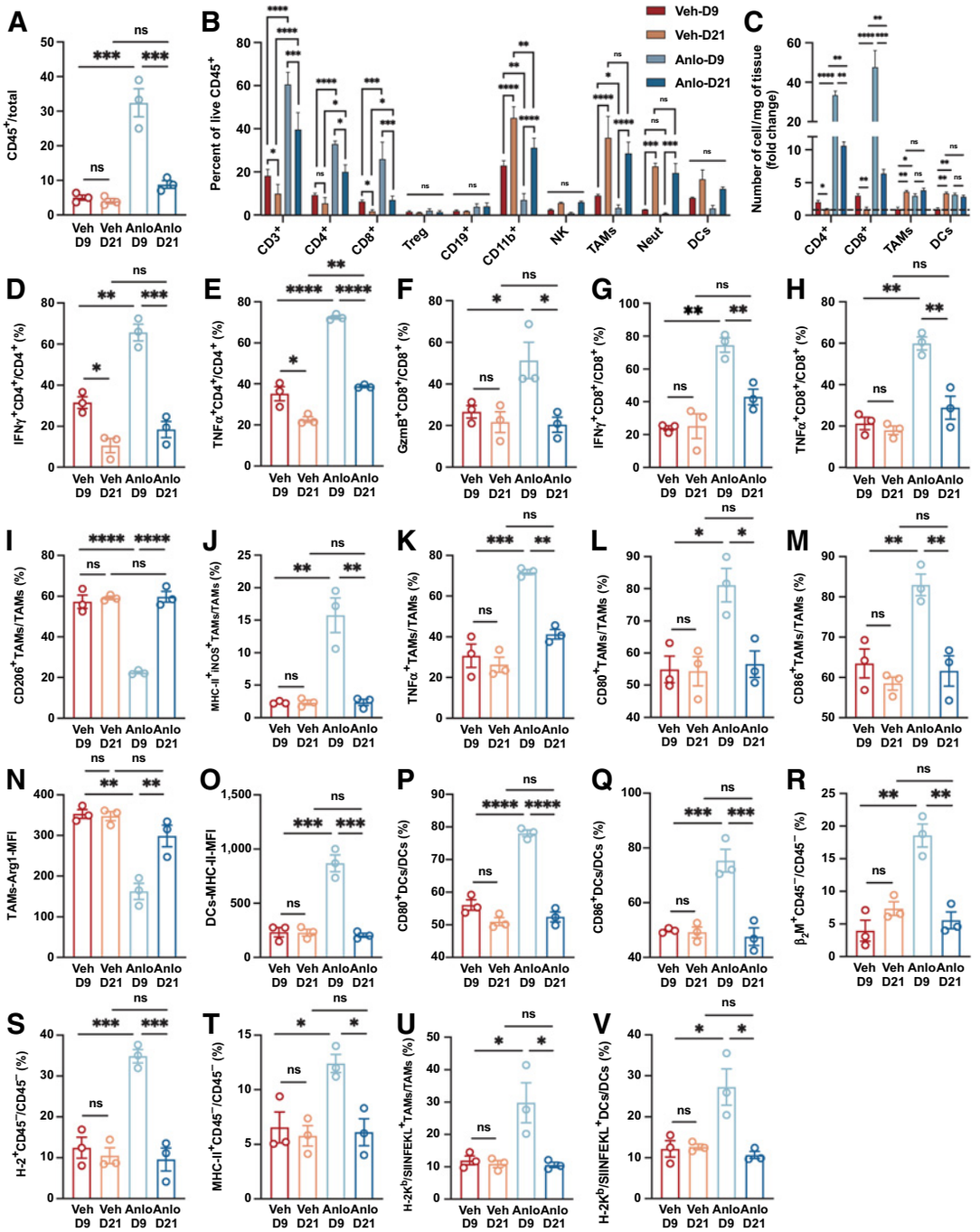

Figure 4.

Anlotinib significantly reprograms the NB immunostimulatory microenvironment, but it is affected by the concomitant period of vascular normalization. **A–V,** Flow cytometry analysis of tumor-infiltrating immune cells and tumor cells in the 975A2 syngeneic mouse model treated with vehicle ± anlotinib (6 mg/kg) for 9 and 21 days as described in Supplementary Fig. S3A, shown by the percentage of parent gates (**A–B**, **D–M**, and **P–V**). MFI indicates the mean fluorescence intensity of the indicated marker (**N–O**). Major immune cell panel, including leukocytes, $CD3^+$ T cells, $CD4^+$ T cells, $CD8^+$ T cells, Tregs, B cells, NK cells, TAMs, neutrophils, and DCs (**A–B**). Fold change relative to the vehicle mean (D9 or D21) in total cell abundance (cells/mg, **C**). T-cell function panel, including the expression of IFNγ, TNFα, and GzmB on T cells (**D–H**). TAM function panel, including the expression of CD206, MHC-II, iNOS, TNFα, costimulatory molecules (CD80 and CD86), and Arg1 on TAMs (**I–N**). DC function panel, including the expression of MHC-II and costimulatory molecules (CD80 and CD86) on DCs (**O–Q**). Tumor cell panel, including the expression of β_2M, H-2, and MHC-II on tumor cells (**R–T**). Antigen cross-presentation panel, including the expression of H-$2K^b$/SIINFEKL on TAMs and DCs (**U–V**). Each dot represents one mouse. $n = 3$ per group. Error bars, mean ± SEM; *, $P < 0.05$; **, $P < 0.01$; ***, $P < 0.001$; ****, $P < 0.0001$, two-way ANOVA (**A–V**).

increased expression of MHC-I and MHC-II in NB cells cultured *in vitro* (Supplementary Fig. S3F). The expression of these genes may be induced by IFNγ secreted by T cells after activation (22, 25). Namely, both the numbers and functions of T cells, TAMs, and DCs were significantly improved, and the antigen processing and presentation of tumor cells were also significantly enhanced. To analyze antigen-specific immune responses after anlotinib treatment, we established 975A2-OVA and 9464D-OVA NB models. After treatment with anlotinib, the proportions of TAMs and DCs that cross-presented the MHCI-restricted, OVA-derived SIINFEKL peptide were increased, which may be conducive to the activation of tumor-specific $CD8^+$ T cells (**Fig. 4U** and **V**). TAMs and DCs primarily stimulate $CD4^+$ T-cell functions through MHC-II–mediated antigen presentation (26). These results here showed that anlotinib reprograms the intratumor immune cell compartment toward increased tumor antigen presentation and T cell activation. Notably, the proportions and

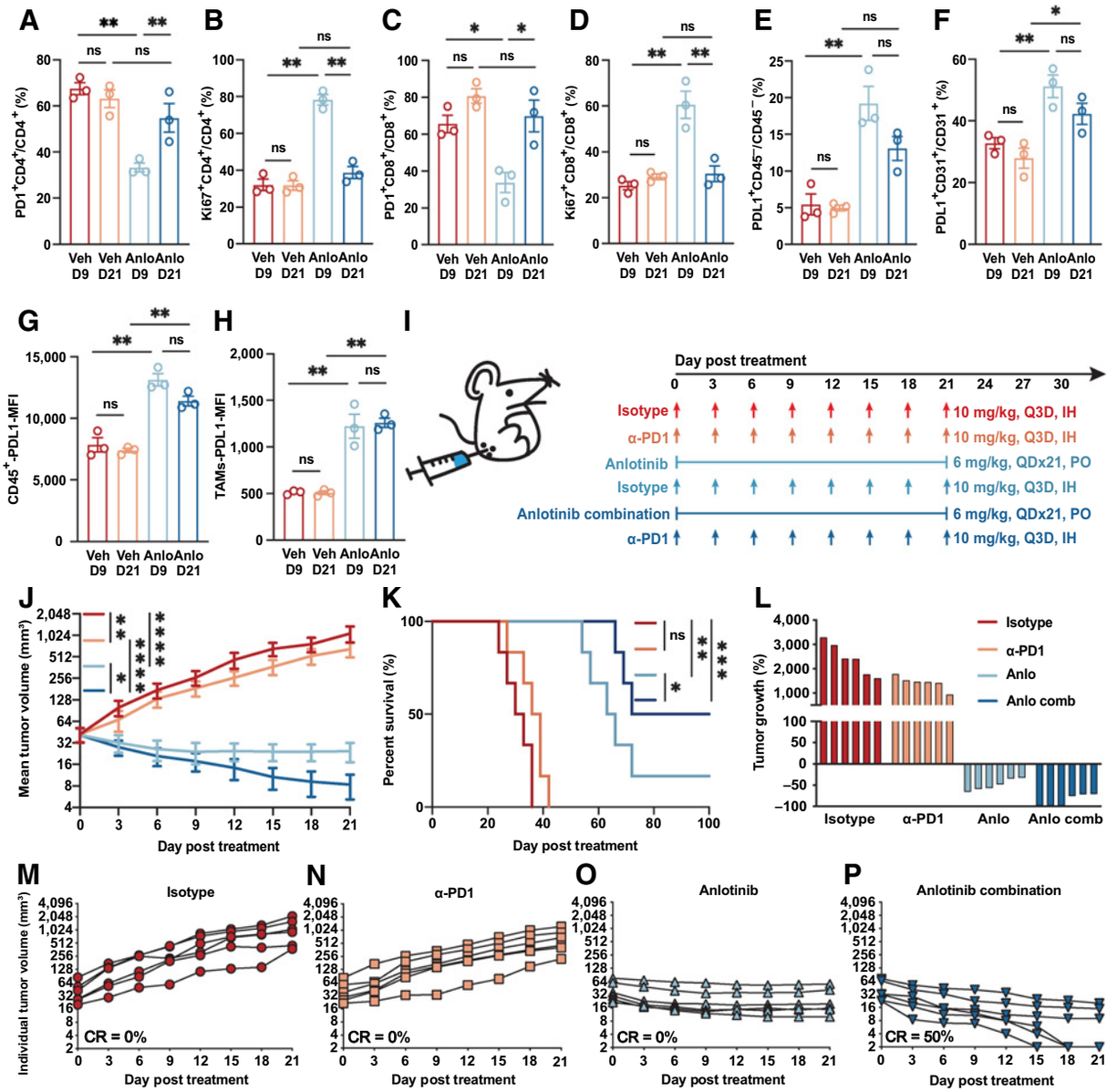

Figure 5.

Efficacy of anlotinib combined with PD-1 checkpoint blockade in the treatment of NB models. **A–H,** Flow cytometry analysis of PD-1 and Ki67 expression on tumor-infiltrating T cells and PD-L1 expression on tumor cells, ECs, and immune cells in the 975A2 syngeneic mouse model treated with vehicle ± anlotinib (6 mg/kg) for 9 days and 21 days as described in Supplementary Fig. S3A, shown by the percentage of parent gates (**A–F**). MFI indicates the mean fluorescence intensity of the indicated marker (**G–H**). Each dot represents one tumor. $n = 3$ per group. **I,** Schematic of the experimental design in NB syngeneic mouse models, $n = 6$ per group. **J** and **K,** Mean tumor volume growth curves and survival curves. Median (50%) survival (after treatment): Isotype control, 31.5 days; α-PD1, 37.5 days; Anlo, 64.5 days; and Anlo + α-PD1, 86 days (**K**). **L,** Change in tumor volume compared with baseline. **M–P,** Individual tumor volume growth curves. Error bars represent the mean ± SEM; *, $P < 0.05$; **, $P < 0.01$; ***, $P < 0.001$; ****, $P < 0.0001$, two-way ANOVA (**A–H** and **J**), log-rank test (**K**).

densities of tumor-infiltrating $CD45^+$ immune cells including $CD4^+$ and $CD8^+$ T cells, their abilities to secrete IFNγ, TNFα, GzmB, the proportion of M1 TAMs, the expression levels of H-$2K^b$/SIINFEKL (antigen cross-presentation), MHC-II and costimulatory molecules on TAMs and DCs, and the expression levels of MHC-I and MHC-II in NB cells were all significantly reduced, but the proportions of M2 TAMs and neutrophils were both increased significantly on day 21 compared with day 9 in the treatment group (**Fig. 4A–V**). Consistent results were obtained in the 975A2 (**Fig. 4**) and 9464D (Supplementary Fig. S4) syngeneic mouse models, indicating that anlotinib significantly reprograms the NB immunostimulatory microenvironment, but it is affected by the concomitant period of vascular normalization. The main flow cytometry gating scheme is shown in Supplementary Fig. S5.

Treatment of NB with anlotinib effectively prevents systemic immunosuppression, but it is also affected by the period of vascular normalization

Tumor cells in the TME release immunosuppressive factors such as VEGF, transforming growth factor β (TGFβ), and prostaglandin E2 (PGE2) into the circulation, resulting in systemic immunosuppression (6). Therefore, we dynamically detected the changes in the total number and proportion of immune cells in the spleen of the tumor-bearing mice (days 9 and 21) and found that the number of total splenocytes of mice in the vehicle group increased significantly on day 21 compared with day 9 (Supplementary Figs. S6A and S7A), potentially reflecting increased tumor burden (Supplementary Figs. S6B and S7B). The proportions of $CD4^+$ and $CD8^+$ T cells in the spleen and peripheral blood were significantly reduced, and the proportion of $CD11b^+$ cells increased, indicating that systemic immunity was suppressed in these mice (Supplementary Fig. S6C and S6D; Supplementary Fig. S7C and S7D). We also analyzed the function of $CD4^+$ and $CD8^+$ T cells in the spleen of mice, namely, their abilities to secrete IFNγ, TNFα, and GzmB. Compared with the treatment group on day 9, the abilities of $CD4^+$ T cells to secrete IFNγ and $CD8^+$ T cells to secrete IFNγ and GzmB in the treatment group were significantly decreased on day 21 (Supplementary Fig. S6E–S6I; Supplementary Fig. S7E–S7I), which was consistent with the results of dynamic observations in the TME and may also be affected by the period of vascular normalization. We included a total of 10 mice in the vehicle group on days 9 and 21, analyzed the correlation between the tumor weight and the proportions of $CD4^+$, $CD8^+$, and $CD11b^+$ cells infiltrated in the TME and spleen, and found that the suppression of the tumor immune microenvironment and systemic immunity by NB was closely related to the tumor size, that is, the larger the tumor was, the lower the proportions of $CD4^+$ and $CD8^+$ T cells, and the higher the proportion of $CD11b^+$ cells (Supplementary Fig. S6N–S6S; Supplementary Fig. S7N–S7S). Further analysis revealed that the proportions of splenic and peripheral blood $CD4^+$ and $CD8^+$ T cells in the treatment groups were significantly higher than that in the vehicle group on day 21, and the proportion of $CD11b^+$ cells decreased (Supplementary Fig. S6C and S6D; Supplementary Fig. S7C and S7D). Thus, it is tempting to speculate that anlotinib effectively prevented systemic immunosuppression possibly by reducing the tumor burden.

Dynamic changes in PD-1 and PD-L1 expression levels during treatment of NB with anlotinib

Although anlotinib reprogrammed the NB immunostimulatory microenvironment and inhibited tumor growth to prolong survival, it did not induce the regression of NB. Therefore, the occurrence of immunosuppressive mechanisms may restrict complete anlotinib-induced antitumor immunity. Based on accumulating evidence, myeloid cells, namely, macrophages, neutrophils, and their subsets, are a source of immunosuppression in the TME (27, 28). However, immunosuppression may also be due to the mechanism of negative feedback regulation of activated adaptive immune cells, such as the upregulation of immune-checkpoint expression (for example, PD-L1) in response to IFNγ secreted by T cells (25, 29, 30). Therefore, we dynamically observed the expression levels of PD-1 and Ki67 on splenic and tumor-infiltrating $CD4^+$ and $CD8^+$ T cells and PD-L1 on tumor cells, immune cells, and tumor ECs. The levels of PD-1 expressed on tumor-infiltrating $CD4^+$ and $CD8^+$ T cells in the treatment group were significantly lower than those in the vehicle group, and the expression levels of Ki67 in these cells were significantly increased on day 9 (**Fig. 5A–D**; Supplementary Fig. S8A). However, the levels of PD-1 expressed on splenic and tumor-infiltrating $CD4^+$ and $CD8^+$ T cells in the treatment group were increased, and the expression levels of Ki67 in these cells were decreased on day 21 (**Fig. 5A–D**; Supplementary Fig. S6J–S6M; Supplementary Fig. S7J–S7M; Supplementary Fig. S8A). In combination with the aforementioned results, the numbers of tumor-infiltrating $CD4^+$ and $CD8^+$ T cells and the abilities of tumor-infiltrating and splenic $CD4^+$ and $CD8^+$ T cells to secrete IFNγ, TNFα, and GzmB were significantly reduced in the treatment group on day 21 compared with day 9 (**Fig. 4B–H**; Supplementary Figs. S4B–S4H, S6E–S6I, and S7E–S7I), indicating that the function of T cells had begun to be inhibited. No significant differences in the expression levels of PD-L1 on tumor cells, immune cells, and ECs were observed between the treatment groups on days 9 and 21, but PD-L1 was expressed at significantly higher levels in the treatment group than in the vehicle group at both time points (**Fig. 5E–H**; Supplementary Fig. S8B and S8C). These results indicate a potentially immunosuppressive mechanism, namely, the increase in tumor and nontumor expression of PD-L1 induced by the activation of T cells mediated by antiangiogenesis.

Efficacy of anlotinib combined with PD-1 checkpoint blockade in the treatment of NB syngeneic mouse models

We then inferred that blocking PD-L1/PD-1 signaling can prevent the early exhaustion of T cells promoted by anlotinib through a counterregulatory mechanism involving enhanced production of IFNγ in the TME. Therefore, we tested anlotinib combined with a PD-1 checkpoint inhibitor treatment in NB syngeneic mouse models. Although the addition of an anti–PD-1 monoclonal antibody (mAb) provided only minimal benefits on top of the substantial antitumoral activity of anlotinib in NB syngeneic mouse models in terms of tumor volumes, the combination of the two resulted in complete remission (CR) rate of 50% in the 975A2 syngeneic mouse model and a partial remission (PR) rate of 50% in the 9464D syngeneic mouse model and significantly prolonged survival (**Fig. 5I–P**; Supplementary Fig. S8D–S8F). Thus, the magnitude of the therapeutic benefit obtained by combining anlotinib with PD-1 checkpoint blockade may vary with the tumor model. Notably, anti–PD-1 monotherapy exerted a very weak therapeutic effect and did not produce significant survival benefits in NB syngeneic mouse models. We observed the effect of combination therapy on tumor-infiltrating immune cells and tumor cells. The results showed that (i) the proportions and densities of tumor-infiltrating $CD45^+$ immune cells, including $CD4^+$ and $CD8^+$ T cells, were significantly increased; (ii) the proportions of TAMs and neutrophils decreased significantly (**Fig. 6A–C**; Supplementary Fig. S8G–S8I); (iii) the abilities of $CD4^+$ and $CD8^+$ T cells to secrete IFNγ, TNFα, and GzmB were significantly enhanced (**Fig. 6D–H**; Supplementary Fig. S8J

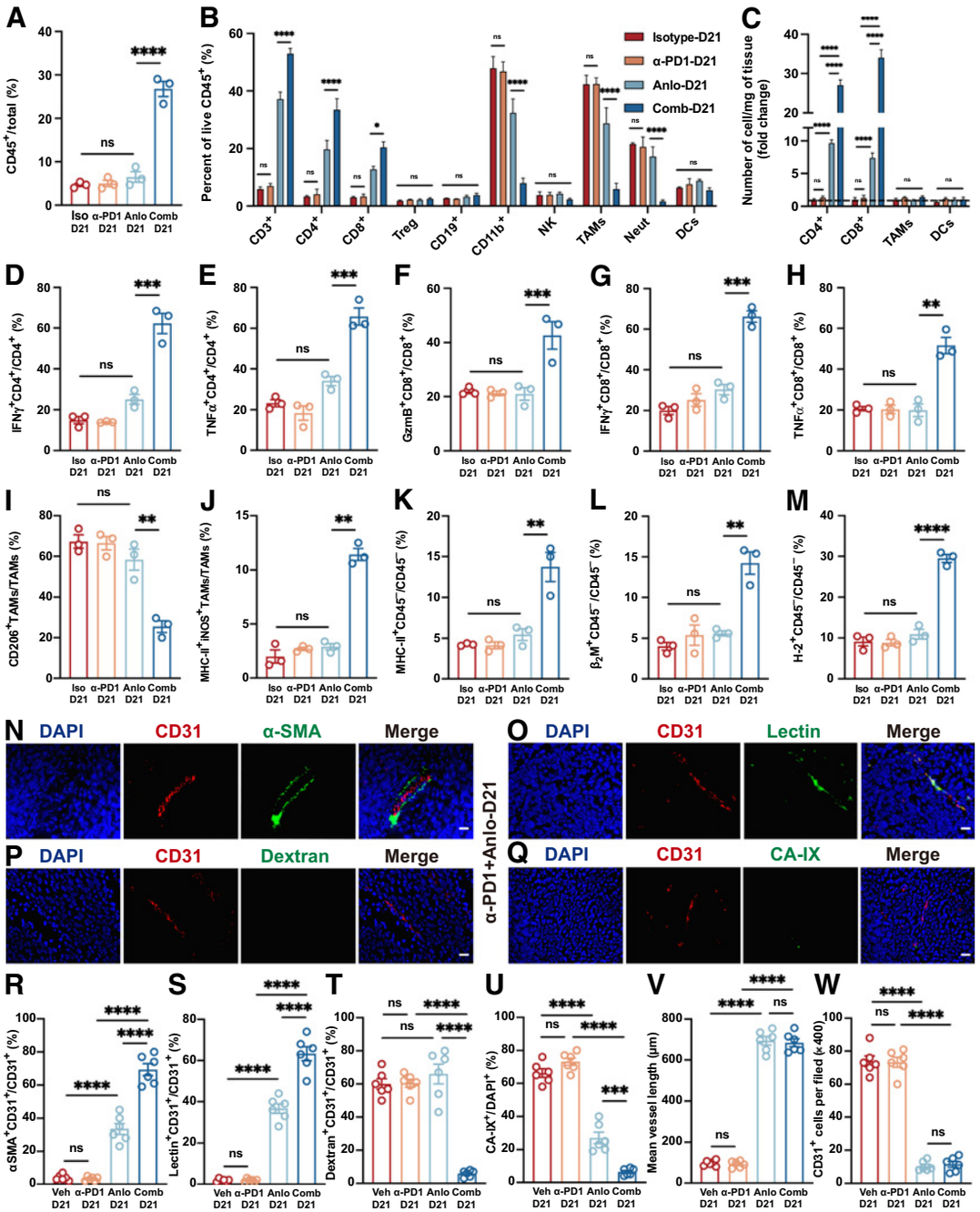

Figure 6.

Anlotinib combined with PD-1 checkpoint blockade prolongs the period of vascular normalization. **A–M,** Flow cytometry analysis of tumor-infiltrating immune cells and tumor cells in 975A2 syngeneic mouse model treated as described in **Fig. 5I**, shown by the percentage of parent gates (**A–B** and **D–M**). Major immune cell panel, including leukocytes, $CD3^+$ T cells, $CD4^+$ T cells, $CD8^+$ T cells, Tregs, B cells, NK cells, TAMs, neutrophils, and DCs (**A–B**). Fold change relative to the vehicle mean (D9 or D21) in total cell abundance (cells/mg, **C**). T-cell function panel, including the expression of IFNγ, TNFα, and GzmB on T cells (**D–H**). TAM function panel, including the expression of CD206, MHC-II, and iNOS on TAMs (**I–J**). Tumor cell panel, including the expression of MHC-II, β_2M, and H-2 on tumor cells (**K–M**). Each dot represents one tumor. $n = 3$ per group. **N–Q,** Representative immunofluorescence images of CD31 (red), α-SMA, lectin, dextran, and CA-IX (green), and DAPI (blue) staining of tumor tissues in NB syngeneic mouse models treated with anlotinib combined with an anti–PD-1 antibody for 21 days as described in **Fig. 5I**. Scale bars, 100 μm. **R–W,** Quantitation results of immunofluorescent images (**N–Q**). Relative proportions of α-SMA^+ pericyte-covered blood vessels (**R**), $lectin^+$ blood vessels (**S**), $dextran^+$ blood vessels (**T**), and $CA\text{-}IX^+$ cells (**U**) in NB syngeneic mouse models treated as described in **Fig. 5I**. Relative tumor vessel length (**V**) and number of $CD31^+$ cells (**W**) in NB syngeneic mouse models treated as described in **Fig. 5I**. Each dot indicates one tumor and represents the average of five images. $n = 6$ per group, including 975A2 ($n = 3$) and 9464D ($n = 3$). Error bars represent the mean ± SEM; *, $P < 0.05$; **, $P < 0.01$; ***, $P < 0.001$; ****, $P < 0.0001$, two-way ANOVA (**A–M** and **R–W**).

and S8K); (iv) the proportion of M1 TAMs increased and the proportion of M2 TAMs decreased (**Fig. 6I** and **J**; Supplementary Fig. S8L); and (v) the expression levels of MHC-I and MHC-II in NB cells were significantly increased in the combined treatment group on day 21 (**Fig. 6K–M**; Supplementary Fig. S8M).Compared with the anlotinib monotherapy group on day 21, the pericyte coverage and vascular perfusion were significantly increased, vascular leakage was reduced, and hypoxia was alleviated in the combined treatment group (**Fig. 6N–W**). Together, our findings in NB syngeneic mouse models illustrate the potential benefits of combining anlotinib with PD-1 checkpoint blockade.

Anlotinib induces tumor vessel normalization at least partially through CD4$^+$ T cells, and its combination with an anti–PD-1 antibody prolongs the period of vascular normalization

Collectively, our results indicate that innate and adaptive immune cells, especially T cells, play a role in the antitumor activity of anlotinib. It is worth noting that a study has shown that CD4$^+$ T cells increase the coverage of pericytes in an IFNγ-dependent manner, subsequently mediating vessel normalization and further increasing the infiltration of immune cells (10). Therefore, mutual regulation may exist between tumor vascular normalization and immunostimulatory reprogramming in NB. To formally establish their involvement, we depleted CD4$^+$ or CD8$^+$ T cells from NB tumor-bearing mice using anti-CD4 or anti-CD8 mAb. Mice bearing early established tumors were treated with the corresponding antibody every three days starting six days before anlotinib treatment (Supplementary Fig. S9Q). Anti-CD4 and anti-CD8 treatments effectively depleted the CD4$^+$ and CD8$^+$ T cells in the peripheral blood of tumor-bearing mice, respectively, and both reduced the beneficial effect of anlotinib on delaying tumor growth and prolonging survival (Supplementary Fig. S9R and S9S; **Fig. 7A–D**). Then, we dynamically observed the effects of depleting CD4$^+$ T cells or CD8$^+$ T cells on the structure and function of tumor vessels by performing immunofluorescence staining (days 9 and 21). Our results showed that the depletion of CD4$^+$ T cells shortened the length of tumor vessels, reduced the coverage of pericytes, decreased vascular perfusion, increased vascular leakage, and exacerbated hypoxia (**Fig. 7E–N**). Notably, the vascular maturity observed after 21 days of treatment with the anti-CD4 antibody in combination with anlotinib was lower than that observed after 9 days, and it was further lower than that in the day 21 anlotinib treatment group (**Fig. 7I–N**), indicating that there is a shifted kinetics in CD4$^+$ T cell–mediated vascular normalization. The depletion of CD8$^+$ T cells had no obvious effect on the structure and function of tumor vessels (**Fig. 7E–N**), consistent with previous findings in breast cancer models (10). We noted, however, it also weakened the efficacy of anlotinib (**Fig. 7A–D**), indicating that the antitumor activity of anlotinib was at least partially CD8$^+$ T cell dependent. Based on these results, we speculate that the combination with PD-1 checkpoint blockade therapy reverses the early exhaustion of CD4$^+$ T cells and ultimately prolongs the period of vascular normalization.

The mechanism of interaction between anlotinib and anti–PD-1 therapy in NB syngeneic mouse models

Anlotinib facilitates tumor vessel normalization by inhibiting proangiogenic factor receptors (VEGFR, PDGFR, and FGFR) and reducing the expression of proangiogenic factors (*Angpt2, Pdgfa*, and *Pdgfb*). The pericyte coverage and perfusion of tumor vessels are increased, and blood vessel leakage and tissue hypoxia are reduced. The expression levels of immune cell adhesion molecules (*Selp, Madcam1*, and *Icam1*) and chemokines and their receptor (*Cxcl9, Cxcl10*, and *Cxcr3*) are increased. The infiltration of immune effector cells is increased, and their functions are enhanced. For example, the infiltration of CD4$^+$ T cells is increased, and their abilities to secrete IFNγ and TNFα are enhanced; the infiltration of CD8$^+$ T cells is also increased, and their abilities to secrete IFNγ, TNFα, and GzmB are enhanced; the proportion of M1 TAMs is increased, and the proportions of M2 TAMs and neutrophils are decreased. The densities of DCs and TAMs are increased, and their antigen presentation function is also enhanced. T cell–derived IFNγ promotes the expression of MHC-I and MHC-II in NB cells and improves antigen processing and presentation. Moreover, IFNγ enhances the expression of PD-L1 in the TME, and combined treatment with an anti–PD-1 antibody reverses the early exhaustion of T cells. Anti–PD-1 immunotherapy and antigen presentation enhance the activation of CD4$^+$ T cells, forming a positive feedback loop of vascular normalization and immunostimulatory reprogramming, thereby prolonging the period of vascular normalization (**Fig. 8**).

Discussion

By performing bioinformatic analysis, Tian and colleagues found that in breast cancer patients, gene-expression characteristics related to vascular normalization are closely related to immune activation pathways, especially the infiltration and activation of T cells. They proved that CD4$^+$ T cells induce tumor vascular normalization in an IFNγ-dependent manner and further increase the infiltration of immune cells (10). Our analysis of patients with NB and LUAD enabled us to draw similar conclusions, and we experimentally verified the results in NB syngeneic mouse models. We found that after anlotinib treatment, tumor vessel normalization occurred, the infiltration of T cells increased, and immune activity was enhanced. Moreover, the depletion of CD4$^+$ T cells leads to a decrease in the degree of vascular normalization, which proves that there is a mutual regulation loop. We also found that anlotinib combined with a PD-1 checkpoint inhibitor treatment of NB prolongs the period of vascular normalization and induces NB regression.

An increasing number of studies have shown that lower doses of single-targeted anti-VEGFA or anti-VEGFR2 drugs may be effective strategies for vascular normalization, whereas higher doses will overprune the vessels to aggravate hypoxia and accelerate the metastasis of malignant tumors (31–33). However, our results show that the therapeutic effect of anlotinib is dose-dependent, which is different from the previous conclusions obtained with single-targeted antiangiogenic drugs. This difference may be due to its inhibitory effects on multiple kinases with diverse activities. In a previous exploration of bevacizumab combined with chemotherapy in the treatment of triple-negative breast cancer, this regimen was shown to prolong PFS but not OS. This means that although it delayed tumor recurrence, there may be problems such as tumor resistance and accelerated growth. Accordingly, the FDA withdrew its approval for breast cancer indications. Several basic studies have found that after effectively inhibiting the activation of the classic VEGFA pathway, the tumor often activates multiple compensatory "bypass activation" pathways, such as the VEGFC (34), TGF (35), and FGF (36) pathways, worsening the biological behavior of tumor cells, as indicated by the invasion of surrounding tissues, the "hijacking" of vessels to support tumor growth (37), or the occurrence of vasculogenic mimicry to increase the supply of blood and oxygen, rendering drugs targeting vascular ECs useless (38). The abovementioned bypass activation mechanisms cause the tumor and its blood vessels to rapidly "rebound" and even lead to an increase in tumor invasiveness and metastasis after

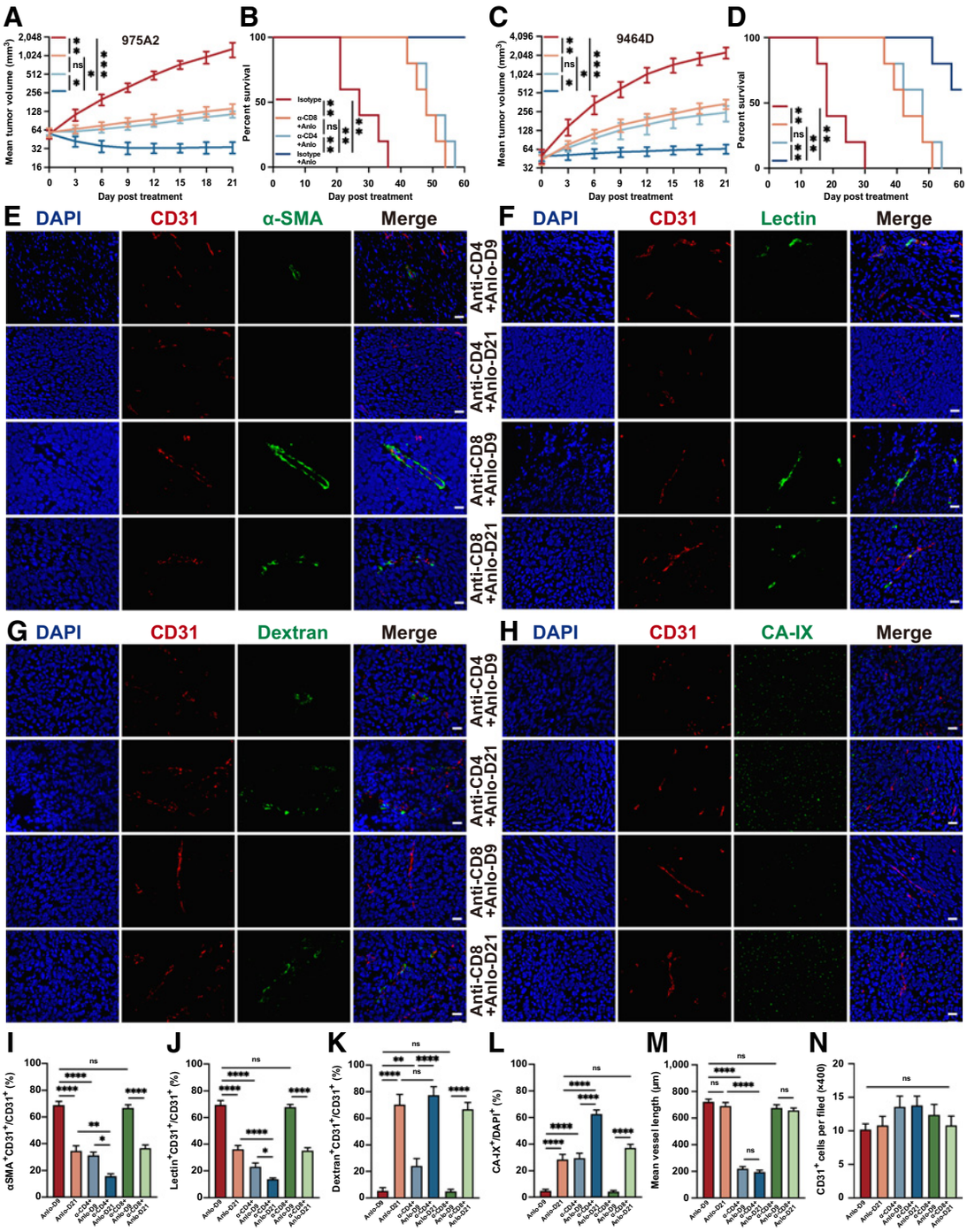

Figure 7.

Anlotinib induces tumor vessel normalization at least partially through $CD4^+$ T cells. **A–D,** Tumor growth curves and survival curves of 975A2 and 9464D syngeneic mouse models treated as described in Supplementary Fig. S9Q ($n = 5$ per group). Median (50%) survival (after treatment): isotype control, 27 days; Anlo + α-CD8, 48 days; Anlo + α-CD4, 48 days; and Anlo, not reached (**B**). Median (50%) survival (after treatment): isotype control, 18 days; Anlo + α-CD8, 42 days; Anlo + α-CD4, 48 days; and Anlo, not reached (**D**). **E–H,** Representative immunofluorescence images of CD31 (red), α-SMA, lectin, dextran and CA-IX (green), and DAPI (blue) staining of tumor tissues in NB syngeneic mouse models treated as described in Supplementary Fig. S9Q. Scale bars, 100 μm. **I–N,** Quantitation results of immunofluorescent images (**E–H**). Relative proportions of α-SMA^+ pericyte-covered blood vessels (**I**), $lectin^+$ blood vessels (**J**), $dextran^+$ blood vessels (**K**), and CA-IX^+ cells (**L**) in NB syngeneic mouse models treated as described in Supplementary Fig. S9Q. Relative tumor vessel length (**M**) and number of $CD31^+$ cells (**N**) in NB syngeneic mouse models treated as described in Supplementary Fig. S9Q. $n = 6$ per group, including 975A2 ($n = 3$) and 9464D ($n = 3$). Error bars represent the mean ± SEM; *, $P < 0.05$; **, $P < 0.01$; ***, $P < 0.001$; ****, $P < 0.0001$, two-way ANOVA (**A**, **C** and **I–N**), log-rank test (**B** and **D**).

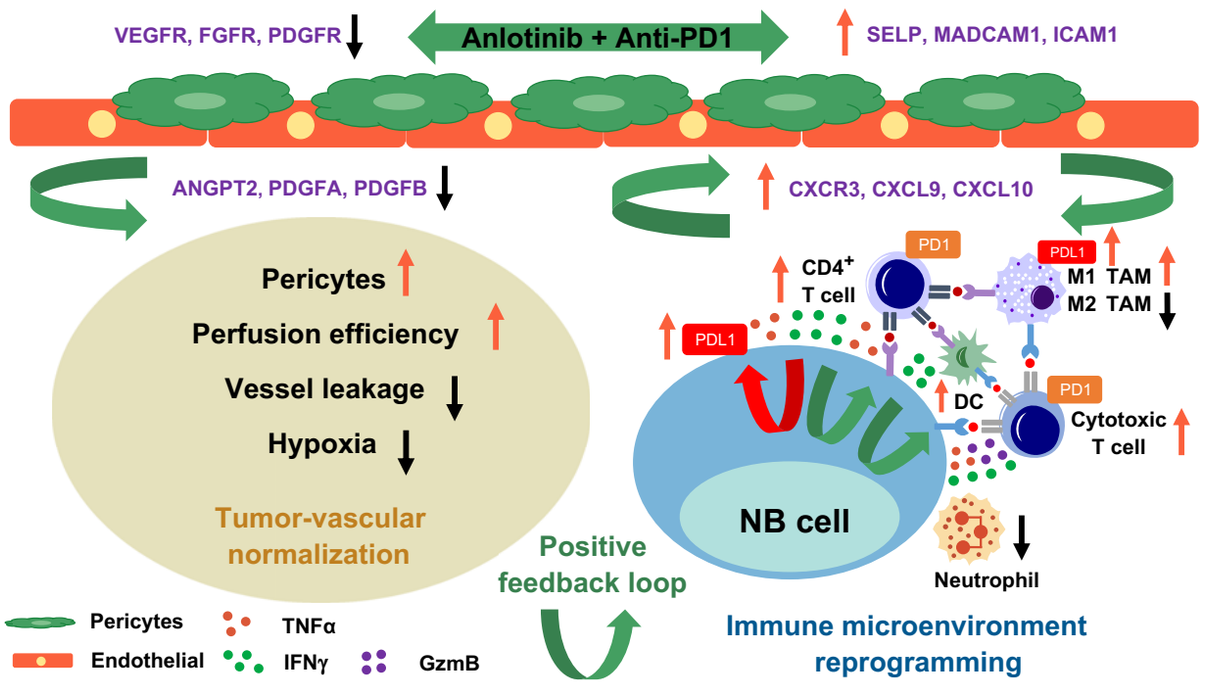

Figure 8.

Schematic of the mechanism of interaction between anlotinib and anti–PD-1 therapy in NB syngeneic mouse models. Anlotinib facilitates tumor vessel normalization by inhibiting proangiogenic factor receptors (VEGFR, PDGFR, and FGFR) and reducing the expression of proangiogenic factors (*Angpt2, Pdgfa*, and *Pdgfb*). The pericyte coverage and perfusion of tumor vessels are increased, and blood vessel leakage and tissue hypoxia are reduced. The expression levels of immune cell adhesion molecules (*Selp, Madcam1*, and *Icam1*) and chemokines and their receptor (*Cxcl9, Cxcl10*, and *Cxcr3*) are increased. The infiltration of immune effector cells is increased, and their functions are enhanced. For example, the infiltration of $CD4^+$ T cells is increased, and their abilities to secrete IFNγ and TNFα are enhanced; the infiltration of $CD8^+$ T cells is also increased, and their abilities to secrete IFNγ, TNFα, and GzmB are enhanced; the proportion of M1 TAMs is increased, and the proportions of M2 TAMs and neutrophils are decreased. The densities of DCs and TAMs are increased, and their antigen presentation function is also enhanced. T cell–derived IFNγ promotes the expression of MHC-I and MHC-II in NB cells and improves antigen processing and presentation. Moreover, IFNγ enhances the expression of PD-L1 in the TME, and combined treatment with an anti–PD-1 antibody reverses the early exhaustion of T cells. Anti–PD-1 immunotherapy and antigen presentation enhance the activation of $CD4^+$ T cells, forming a positive feedback loop of vascular normalization and immunostimulatory reprogramming, thereby prolonging the period of vascular normalization.

treatment. Therefore, bypass activation in tumor vascular ECs after inhibiting the main angiogenesis signaling pathway has become an important cause of drug resistance. The new generation antiangiogenic drug anlotinib targets angiogenesis pathways, including those of VEGFR, FGFR, and PDGFR, and targets the stem cell factor receptor c-KIT (13). Its multitarget mechanism leads to significant curative effects, prolongs the PFS and OS of patients with advanced NSCLC, and ends the history of refractory lung cancer patients with no medicines available (14). We have reported a patient with advanced LUAD harboring a *KRAS* mutation who was treated with anlotinib after multiline chemotherapy and radiotherapy progression. The PFS was up to 21 months, and the OS was up to 5.5 years (39).

Among a variety of angiogenic molecules, the roles of VEGF in systemic and local immunosuppression have been extensively studied in tumor models. Increased VEGF levels in the TME directly inhibit the trafficking, proliferation, and effector function of T cells by altering the expression of adhesion molecules, such as intercellular adhesion molecule-1 (ICAM1) and vascular cell adhesion molecule-1 (VCAM1; refs. 40, 41). VEGF also inhibits the maturation and antigen presentation function of DCs, thereby preventing T-cell activation and reducing the T cell–mediated anticancer immune response (42, 43). High levels of VEGF can also promote the recruitment and proliferation of immunosuppressive cells, such as Tregs, MDSCs, and protumor, M2-like TAMs (44, 45). VEGF also promotes angiogenesis that results in an abnormal tumor vasculature, leading to hypoxia and a low pH in the TME that in turn promotes local and systemic immunosuppression (6, 46). First, anlotinib inhibited proangiogenic factor receptors (VEGFR, PDGFR, and FGFR), reduced the expression of proangiogenic factors (*Angpt2, Pdgfa*, and *Pdgfb*), and enhanced the expression of immune cell adhesion molecules (*Selp, Madcam1*, and *Icam1*) and chemokines and their receptor (*Cxcl9, Cxcl10*, and *Cxcr3*). It inhibited tumor angiogenesis and normalized the remaining blood vessels as well, which was related to increased immune cell extravasation into the TME. Second, anlotinib reprogrammed protumor, M2-like TAMs toward an anticancer M1 phenotype, increased the numbers of DCs and TAMs, and enhanced the antigen presentation function. These changes may enhance the uptake, processing, and presentation of tumor-associated antigens to $CD4^+$ and $CD8^+$ T cells, thereby enhancing their activation and expansion. Collectively, anlotinib promotes antitumor immunity through multidimensional effects on both innate and adaptive immune cells and complementary effects on tumor blood vessels. Notably, Allen and colleagues found that the systemic immunosuppression caused by the tumor can be reversed by surgical removal (47). We also observed a similar phenomenon in NB syngeneic mouse models; namely, the suppression of the tumor immune microenvironment and systemic immunity were both closely

related to the tumor size. Thus, it is tempting to speculate that anlotinib effectively prevented systemic immunosuppression, possibly by reducing tumor burden.

A series of preclinical studies have identified a period of vessel normalization induced by antiangiogenic therapy, but how to define this period is still inconclusive. Studies have shown that the normalization of tumor vessels may occur within one day in mice and humans, lasting approximately 2–10 days in mice and several months in humans, depending on the type of tumor and the application dose, time, and type of antiangiogenic drugs (48–50). There are cases in which antiangiogenic drugs excessively destroy tumor vessels in a dose- and time-dependent manner, leading to hypoxia and immunosuppression. Therefore, we dynamically observed TME changes at a dose of 6 mg/kg, fully considered the dose and time of anlotinib, looked for its resistance mechanism, and further explored its combined treatment strategies. We dynamically analyzed the features of the tumor vessels after anlotinib treatment using immunofluorescence staining. Compared with the treatment group on day 9, the coverage of pericytes and vascular perfusion were decreased, vascular leakage was increased, and hypoxia was aggravated in the monotherapy group on day 21. The results of dynamic observation of the TME using flow cytometry further confirmed the existence of the period of vessel normalization. Interestingly, we detected increased expression levels of PD-1 on splenic and tumor-infiltrating $CD4^+$ and $CD8^+$ T cells and decreased expression levels of Ki67 in these cells on day 21 compared with day 9 in the anlotinib treatment group. Simultaneously, the numbers of tumor-infiltrating $CD4^+$ and $CD8^+$ T cells and the abilities of tumor-infiltrating and splenic $CD4^+$ and $CD8^+$ T cells to secrete IFNγ, TNFα, and GzmB were significantly reduced on day 21 compared with day 9 in the anlotinib treatment group, indicating that T cells had begun to be inhibited. After anlotinib treatment, the upregulation of PD-L1 was observed on tumor cells, ECs, and immune cells. Therefore, although high PD-1 expression is a marker of T-cell activation, it is also of the "exhausted" phenotype of effector T cells.

In fact, the findings of multiple preclinical studies have provided evidence of the efficacy of combining antiangiogenic therapy with ICIs (6, 41). For example, in various cancer models, an anti–PD-1 antibody combined with anti–ANG2-VEGF antibody improved the degree of tumor control. The findings reported by Schmittnaegel and colleagues are consistent with our observation that effective antiangiogenic therapy increases the number of activated T cells but also induces PD-L1 expression in the TME, likely through T cell–derived IFNγ (30). Collectively, strong reasons exist to support the combination of anlotinib and PD-1 checkpoint blockade. We found that anlotinib combined with PD-1 checkpoint blockade reversed the early exhaustion of T cells, extended the period of vascular normalization, and finally induced NB regression. An important factor is to determine whether this preclinical research will translate into patient benefits. Currently, immunotherapy is only effective for a small number of patients with lung cancer, and the overall effective rate is less than 20% (51). A phase I clinical study (NCT03628521) on the efficacy and safety of anlotinib combined with sintilimab as the first-line treatment of advanced NSCLC included 22 patients with unresectable stage IIIB/C or stage IV NSCLC who did not receive treatment and did not have *EGFR/ALK/ROS1* mutations; 16 patients achieved PR, and six patients reached stable disease; the objective response rate was 72.7%, the disease control rate was 100%, and the median PFS was 15 months. A subgroup analysis based on PD-L1 expression and the tumor mutation burden of patients at baseline showed that the combination therapy displayed consistent efficacy in each subgroup (52). Based on the encouraging efficacy, tolerability, and safety, phase II clinical trials with expanded sample sizes were successively conducted. Anlotinib combined with sintilimab may become a new choice for the first-line chemotherapy-free treatment of advanced NSCLC. The new clinical data and the results of this study show that the combined use of anlotinib and PD-1 checkpoint blockade therapy may transform "cold tumors" into "hot tumors." It may represent a new treatment option not only for lung cancer but also for other malignant tumors, including NB.

Conclusions

In summary, we proved that GPAGs are associated with vessel normalization and T-cell activation in patients with NB. Then, we used NB syngeneic mouse models to prove that anlotinib induces tumor vessel normalization at least partially through $CD4^+$ T cells, reprograms the immunosuppressive TME into an immunostimulatory TME, significantly inhibits tumor growth, and effectively prevents systemic immunosuppression. Moreover, anlotinib improves the response to immunotherapy. The combination of anlotinib with a PD-1 checkpoint inhibitor counteracts the immunosuppression caused by the upregulation of PD-L1 in the TME after monotherapy, thereby reversing the early exhaustion of $CD4^+$ T cells, prolonging the period of vascular normalization, and finally inducing NB regression. To our knowledge, this study is the first to dynamically evaluate the effect of a multitarget antiangiogenic tyrosine kinase inhibitor on the tumor immune microenvironment. These findings have important clinical value in guiding the testing of related drugs in patients with NB and other cancers. Based on the aforementioned basic research findings, we are conducting a phase II clinical study (NCT04842526) on the efficacy and safety of anlotinib, irinotecan, and temozolomide in the treatment of refractory or relapsed NB, and we hope to observe patient benefit. Anlotinib, which was first developed in China, is a promising agent that provides hope for the medical community around the world and the field of oncology. We anticipate that it will be applied to treat more cancers in the future.

Authors' Disclosures

No disclosures were reported.

Authors' Contributions

Y. Su: Conceptualization, data curation, formal analysis, validation, investigation, visualization, methodology, writing–original draft, writing–review and editing. **B. Luo:** Software and visualization. **Y. Lu:** Investigation. **D. Wang:** Resources. **J. Yan:** Resources. **J. Zheng:** Resources. **J. Xiao:** Resources. **Y. Wang:** Investigation. **Z. Xue:** Investigation. **J. Yin:** Investigation. **P. Chen:** Investigation. **L. Li:** Conceptualization, supervision, validation, project administration, writing–review and editing. **Q. Zhao:** Conceptualization, supervision, funding acquisition, project administration, writing–review and editing.

Acknowledgments

We acknowledge Professor Dr. Rimas Orentas (Seattle Children's Research Institute) for sharing the 975A2 and 9464D cell lines. We thank Professor Deqing Hu (Department of Cell Biology at Tianjin Medical University) for sharing the recombinant lentiviral vector pLV-OVA-Flag-IRES-GFP. We thank Mr. Deng Liu and Ms. Aidi Lv (Chia Tai Tianqing Pharmaceutical Group Co., Ltd) for providing anlotinib. We thank Ms. Xuzhen Zhang (Basic Research Center of Tianjin Medical University) for providing technical assistance with flow cytometry. This work was supported by funding from the National Key Research and Development Program of China (No. 2018YFC1313000, 2018YFC1313001, and 2018YFC1313002).

The costs of publication of this article were defrayed in part by the payment of page charges. This article must therefore be hereby marked *advertisement* in accordance with 18 U.S.C. Section 1734 solely to indicate this fact.

Received June 21, 2021; revised October 12, 2021; accepted November 22, 2021; published first November 29, 2021.

References

1. Pinto NR, Applebaum MA, Volchenboum SL, Matthay KK, London WB, Ambros PF, et al. Advances in risk classification and treatment strategies for neuroblastoma. J Clin Oncol 2015;33:3008–17.
2. Matthay KK, Maris JM, Schleiermacher G, Nakagawara A, Mackall CL, Diller L, et al. Neuroblastoma. Nat Rev Dis Primers 2016;2:16078.
3. Shen X, Zhao B. Efficacy of PD-1 or PD-L1 inhibitors and PD-L1 expression status in cancer: meta-analysis. BMJ 2018;362:k3529.
4. Casey DL, Cheung NV. Immunotherapy of pediatric solid tumors: treatments at a crossroads, with an emphasis on antibodies. Cancer Immunol Res 2020;8: 161–6.
5. Wienke J, Dierselhuis MP, Tytgat GAM, Kunkele A, Nierkens S, Molenaar JJ. The immune landscape of neuroblastoma: challenges and opportunities for novel therapeutic strategies in pediatric oncology. Eur J Cancer 2021;144:123–50.
6. Fukurnura D, Kloepper J, Amoozgar Z, Duda DG, Jain RK. Enhancing cancer immunotherapy using antiangiogenics: opportunities and challenges. Nat Rev Clin Oncol 2018;15:325–40.
7. Jain RK. Antiangiogenesis strategies revisited: from starving tumors to alleviating hypoxia. Cancer Cell 2014;26:605–22.
8. Jain RK. Normalizing tumor microenvironment to treat cancer: bench to bedside to biomarkers. J Clin Oncol 2013;31:2205–18.
9. Palucka AK, Coussens LM. The basis of oncoimmunology. Cell 2016;164: 1233–47.
10. Tian L, Goldstein A, Wang H, Lo HC, Kim IS, Welte T, et al. Mutual regulation of tumour vessel normalization and immunostimulatory reprogramming. Nature 2017;544:250–4.
11. Garcia J, Hurwitz HI, Sandler AB, Miles D, Coleman RL, Deurloo R, et al. Bevacizumab (Avastin (R)) in cancer treatment: a review of 15 years of clinical experience and future outlook. Cancer Treat Rev 2020;86:102017.
12. Modak S, Kushner BH, Basu E, Roberts SS, Cheung NKV. Combination of bevacizumab, irinotecan, and temozolomide for refractory or relapsed neuroblastoma: results of a phase II study. Pediatr Blood Cancer 2017;64:10.1002/pbc.26448.
13. Shen GS, Zheng FC, Ren DF, Du F, Dong QX, Wang ZY, et al. Anlotinib: a novel multi-targeting tyrosine kinase inhibitor in clinical development. J Hematol Oncol 2018;11:120.
14. Han B, Li K, Wang Q. Effect of anlotinib as a third-line or further treatment on overall survival of patients with advanced non-small cell lung cancer: the ALTER 0303 phase 3 clinical trial (vol 4, pg 1569, 2018). JAMA Oncol 2018;4:1625.
15. Chi YHBL, Fang ZW, Hong XN, Yao Y, Sun P, Wang GW, et al. Safety and efficacy of anlotinib, a multikinase angiogenesis inhibitor, in patients with refractory metastatic soft-tissue sarcoma. Clin Cancer Res 2018;24:5233–8.
16. Li D, Chi Y, Chen X, Ge M, Zhang Y, Guo Z, et al. Anlotinib in locally advanced or metastatic medullary thyroid carcinoma: a randomized, double-blind phase IIB trial. Clin Cancer Res 2021;27:3567–75.
17. Ma J, Song Y, Shou J, Bai Y, Li H, Xie X, et al. Anlotinib for patients with metastatic renal cell carcinoma previously treated with one vascular endothelial growth factor receptor-tyrosine kinase inhibitor: a phase 2 trial. Front Oncol 2020;10:664.
18. Ritchie ME, Phipson B, Wu D, Hu YF, Law CW, Shi W, et al. limma powers differential expression analyses for RNA-sequencing and microarray studies. Nucleic Acids Res 2015;43:e47.
19. Yu GC, Wang LG, Han YY., He QY. clusterProfiler: an R package for comparing biological themes among gene clusters. OMICS 2012;16:284–7.
20. Weiss WA, Aldape K, Mohapatra G, Feuerstein BG, Bishop JM. Targeted expression of MYCN causes neuroblastoma in transgenic mice. EMBO J 1997;16:2985–95.
21. Terrile M, Bryan K, Vaughan L, Hallsworth A, Webber H, Chesler L, et al. miRNA expression profiling of the murine TH-MYCN neuroblastoma model reveals similarities with human tumors and identifies novel candidate MiRNAs. PLoS One 2011;6:e28356.
22. Kroesen M, Nierkens S, Ansems M, Wassink M, Orentas RJ, Boon L, et al. A transplantable TH-MYCN transgenic tumor model in C57Bl/6 mice for preclinical immunological studies in neuroblastoma. Int J Cancer 2014;134: 1335–45.
23. Shukla A, Cano-Mejia J, Andricovich J, Burga RA, Sweeney EE, Fernandes R. An engineered prussian blue nanoparticles-based nanoimmunotherapy elicits robust and persistent immunological memory in a TH-MYCN neuroblastoma model. Adv Nanobiomed Res 2021;1:2100021.
24. Armulik A, Genove G, Betsholtz C. Pericytes: developmental, physiological, and pathological perspectives, problems, and promises. Dev Cell 2011;21:193–215.
25. Parker BS, Rautela J, Hertzog PJ. Antitumour actions of interferons: implications for cancer therapy. Nat Rev Cancer 2016;16:131–44.
26. Palucka K, Banchereau J. Cancer immunotherapy via dendritic cells. Nat Rev Cancer 2012;12:265–77.
27. Hanahan D, Coussens LM. Accessories to the crime: functions of cells recruited to the tumor microenvironment. Cancer Cell 2012;21:309–22.
28. Sica A, Bronte V. Altered macrophage differentiation and immune dysfunction in tumor development. J Clin Invest 2007;117:1155–66.
29. Spranger S, Spaapen RM, Zha Y, Williams J, Meng Y, Ha TT, et al. Up-regulation of PD-L1, IDO, and T-regs in the melanoma tumor microenvironment is driven by CD8(+) T cells. Sci Transl Med 2013;5:200ra116.
30. Schmittnaegel M, Rigamonti N, Kadioglu E, Cassara A, Rmili CW, Kiialainen A, et al. Dual angiopoietin-2 and VEGFA inhibition elicits antitumor immunity that is enhanced by PD-1 checkpoint blockade. Sci Transl Med 2017;9: eaak9670.
31. Huang YH, Goel S, Duda DG, Fukumura D, Jain RK. Vascular normalization as an emerging strategy to enhance cancer immunotherapy. Cancer Res 2013;73: 2943–8.
32. Van der Veldt AAM, Lubberink M, Bahce I, Walraven M, de Boer MP, Greuter HNJM, et al. Rapid decrease in delivery of chemotherapy to tumors after anti-VEGF therapy: implications for scheduling of anti-angiogenic drugs. Cancer Cell 2012;21:82–91.
33. Rahbari NN, Kedrin D, Incio J, Liu H, Ho WW, Nia HT, et al. Anti-VEGF therapy induces ECM remodeling and mechanical barriers to therapy in colorectal cancer liver metastases. Sci Transl Med 2016;8:360ra135.
34. Michaelsen SR, Staberg M, Pedersen H, Jensen KE, Majewski W, Broholm H, et al. VEGF-C sustains VEGFR2 activation under bevacizumab therapy and promotes glioblastoma maintenance. Neuro-oncol 2018;20:1462–74.
35. Zhang M, Chu SJ, Zeng FX, Xu HF. Bevacizumab modulates the process of fibrosis in vitro. Clin Exp Ophthalmol 2015;43:173–9.
36. Vila N, Coblentz J, Moreira-Neto C, Bravo V, Zoroquiain P, Burnier MN. Pretreatment of RPE cells with lutein can mitigate bevacizumab-induced increases in angiogenin and bFGF. Ophthalmic Res 2017;57:48–53.
37. Qian CN, Pezzella F. Tumor vasculature: a sally port for inhibiting cancer cell spreading. Cancer Commun 2018;38:52.
38. Wei XX, Chen YH, Jiang XJ, Peng M, Liu YD, Mo YZ, et al. Mechanisms of vasculogenic mimicry in hypoxic tumor microenvironments. Mol Cancer 2021; 20:7.
39. Su Y, Meng Z, Xu X, Wang X, Zuo R, Hou Y, et al. A case report of advanced lung adenocarcinoma harboring KRAS mutation treated with anlotinib. Zhongguo Fei Ai Za Zhi 2018;21:428–30.
40. Dirkx AEM, Egbrink MGAO, Kuijpers MJE, van der Niet ST, Heijnen VVT, Bouma-ter Steege JCA, et al. Tumor angiogenesis modulates leukocyte-vessel wall interactions in vivo by reducing endothelial adhesion molecule expression. Cancer Res 2003;63:2322–9.
41. Khan KA, Kerbel RS. Improving immunotherapy outcomes with anti-angiogenic treatments and vice versa. Nat Rev Clin Oncol 2018;15:310–24.
42. Gabrilovich D, Ishida T, Oyama T, Ran S, Kravtsov V, Nadaf S, et al. Vascular endothelial growth factor inhibits the development of dendritic cells and dramatically affects the differentiation of multiple hematopoietic lineages in vivo. Blood 1998;92:4150–66.
43. Gabrilovich DI, Chen HL, Girgis KR, Cunningham HT, Meny GM, Nadaf S, et al. Production of vascular endothelial growth factor by human tumors inhibits the functional maturation of dendritic cells. Nat Med 1996;2: 1096–103.
44. Hegde S, Leader AM, Merad M. MDSC: markers, development, states, and unaddressed complexity. Immunity 2021;54:875–84.
45. Chaudhary B, Khaled YS, Ammori BJ, Elkord E. Neuropilin 1: function and therapeutic potential in cancer. Cancer Immunol Immun 2014;63:81–99.
46. Huang Y, Yuan J, Righi E, Kamoun WS, Ancukiewicz M, Nezivar J, et al. Vascular normalizing doses of antiangiogenic treatment reprogram the immunosuppressive tumor microenvironment and enhance immunotherapy. Proc Natl Acad Sci U S A 2012;109:17561–6.
47. Allen BM, Hiam KJ, Burnett CE, Venida A, DeBarge R, Tenvooren I, et al. Systemic dysfunction and plasticity of the immune macroenvironment in cancer models. Nat Med 2020;26:1125–34.
48. Winkler F, Kozin SV, Tong RT, Chae SS, Booth MF, Garkavtsev I, et al. Kinetics of vascular normalization by VEGFR2 blockade governs brain tumor response to radiation: role of oxygenation, angiopoietin-1, and matrix metalloproteinases. Cancer Cell 2004;6:553–63.

49. Batchelor TT, Sorensen AG, di Tomaso E, Zhang WT, Duda DG, Cohen KS, et al. AZD2171, a pan-VEGF receptor tyrosine kinase inhibitor, normalizes tumor vasculature and alleviates edema in glioblastoma patients. Cancer Cell 2007;11:83–95.
50. Batchelor TT, Duda DG, di Tomaso E, Ancukiewicz M, Plotkin SR, Gerstner E, et al. Phase II study of cediranib, an oral pan-vascular endothelial growth factor receptor tyrosine kinase inhibitor, in patients with recurrent glioblastoma. J Clin Oncol 2010;28:2817–23.
51. Chae YK, Arya A, Iams W, Cruz MR, Chandra S, Choi J, et al. Current landscape and future of dual anti-CTLA4 and PD-1/PD-L1 blockade immunotherapy in cancer; lessons learned from clinical trials with melanoma and non-small cell lung cancer (NSCLC). J Immunother Cancer 2018;6:39.
52. Chu TQ, Zhong RB, Zhong H, Zhang B, Zhang W, Shi CL, et al. Phase 1b study of sintilimab plus anlotinib as first-line therapy in patients with advanced NSCLC. J Thorac Oncol 2021;16:643–52.